#### RESEARCH ARTICLE

Genome-wide signatures of plastid-nuclear coevolution point to repeated perturbations of plastid proteostasis systems across angiosperms

Evan S. Forsythe, a,1 Alissa M. Williams, and Daniel B. Sloan

<sup>a</sup>Department of Biology, Colorado State University, Fort Collins, Colorado 80523

<sup>1</sup>Corresponding author

**Short title:** Genomic signatures of plastid-nuclear coevolution

**One-sentence summary:** Genome-wide evolutionary rate covariation analyses reveal potential novel plastid-nuclear interactions and suites of coevolving plastid proteostasis genes.

The author responsible for distribution of materials integral to the findings presented in this article in accordance with the policy described in the Instructions for Authors (www.plantcell.org) is: Evan S. Forsythe (esfors@rams.colostate.edu).

#### Abstract

- 2 Nuclear and plastid (chloroplast) genomes experience different mutation rates, levels of
- 3 selection, and transmission modes, yet key cellular functions depend on coordinated interactions
- 4 between proteins encoded in both genomes. Functionally related proteins often show correlated
- 5 changes in rates of sequence evolution across a phylogeny (evolutionary rate covariation or
- 6 ERC), offering a means to detect previously unidentified suites of coevolving and cofunctional
- 7 genes. We performed phylogenomic analyses across angiosperm diversity, scanning the nuclear
- 8 genome for genes that exhibit ERC with plastid genes. As expected, the strongest hits are highly
- 9 enriched for plastid-targeted proteins, providing evidence that cytonuclear interactions affect
- 10 rates of molecular evolution at genome-wide scales. Many identified nuclear genes function in
- 11 post-transcriptional regulation and the maintenance of protein homeostasis (proteostasis),
- including protein translation (in both the plastid and cytosol), import, quality control and
- turnover. We also identified nuclear genes that exhibit strong signatures of coevolution with the
- plastid genome but lack organellar-targeting annotations, making them candidates for having
- previously undescribed roles in plastids. In sum, our genome-wide analyses reveal that plastid-
- 16 nuclear coevolution extends beyond the intimate molecular interactions within chloroplast
- 17 enzyme complexes and may be driven by frequent rewiring of the machinery responsible for
- maintenance of plastid proteostasis in angiosperms.

19 Introduction 20 Only a small fraction of the proteins required for plastid function are encoded by the plastid 21 genome (plastome) itself (Timmis et al., 2004; van Wijk & Baginsky, 2011). The remaining 22 plastid-localized proteins are encoded in the nuclear genome, translated in the cytosol, and 23 imported into plastids (hereafter referred to as nuclear-encoded plastid-targeted [N-pt] proteins), 24 where they often interact with the plastome and its gene products (Gould et al., 2008). These 25 plastid-nuclear interactions are critical for overall fitness, as evidenced by the frequent role of 26 plastid-nuclear incompatibilities in reproductive isolation (Schmitz-Linneweber et al., 2005; Greiner et al., 2011; Bogdanova et al., 2015; Barnard-Kubow et al., 2016; Zupoka et al., 2020). 27 28 29 One signature of proteins that are functionally related and/or coevolving is that they tend to 30 exhibit correlated changes in rates of sequence evolution across a phylogeny, which is known as 31 evolutionary rate covariation (ERC) and can be quantified by comparing genetic distances or 32 branch lengths of gene trees from two potentially interacting genes (Goh et al., 2000; Ramani & 33 Marcotte, 2003; Sato et al., 2005; Clark & Aquadro, 2010; Clark et al., 2012; De Juan et al., 34 2013). The known physical interactions within "chimeric" plastid-nuclear complexes (i.e., those 35 containing both plastome-encoded and N-pt proteins) have provided a valuable system to test 36 and illustrate the principle that coevolution and functional interactions can result in ERC (Sloan 37 et al., 2014; Zhang et al., 2015, 2016; Rockenbach et al., 2016; Weng et al., 2016; Williams et 38 al., 2019). 40 In addition to probing known interactions, ERC has served as a powerful tool to scan entire 41

39

42

43

44

45

46

47

48

49

genomes/proteomes to detect previously unrecognized functional relationships (Findlay et al., 2014; Raza et al., 2019), which do not always entail direct physical interactions (Clark et al., 2012). For example, application of a genome-wide ERC scan in diverse insects with heterogeneous rates of mitochondrial genome evolution recovered novel mitonuclear interactions (Yan et al., 2019). However, despite strong evidence of correlated rates among known members of plastid-nuclear complexes, ERC analysis has not been applied on a genome-wide scale across diverse plant lineages, meaning we may have only scratched the surface with respect to the full breadth of plastid-nuclear interactions. A key barrier is that the frequent occurrence of gene and whole-genome duplication in plants (Panchy et al., 2016; Wendel et al., 2018) makes it

```
50
      inherently difficult to perform phylogenomic scans for ERC. Typical implementations of ERC
51
      analysis require one-to-one orthology in gene trees (Clark et al., 2012; Findlay et al., 2014;
52
      Wolfe & Clark, 2015; Yan et al., 2019), but gene duplication yields large gene families
53
      composed of sequences that share both orthology and paralogy (Bansal & Eulenstein, 2008;
54
      Stolzer et al., 2012). Outside of the context of ERC, numerous studies have overcome challenges
55
      associated with phylogenomics in plants by carefully filtering gene families and/or extracting
56
      subtrees that represent mostly orthologs (Sanderson & McMahon, 2007; Duarte et al., 2010; De
57
      Smet et al., 2013; Sangiovanni et al., 2013; Forsythe et al., 2020). Nevertheless, these approaches
58
      cannot completely eliminate the pervasive effects of gene duplication and differential loss, so
59
      performing ERC analyses across diverse plant lineages requires a novel approach that can
60
      accommodate this recurring history.
61
62
      ERC analyses have the potential to be especially powerful for probing plastid-nuclear
63
      interactions because the rate of plastome evolution can differ greatly across angiosperm species,
64
      with several lineages exhibiting extreme accelerations. Not surprisingly, angiosperms that lose
65
      photosynthetic function and transition to parasitic/heterotrophic lifestyles exhibit massive
      plastome decay and rapid protein sequence evolution (Wicke et al., 2016), in extreme cases
66
67
      resulting in outright loss of the entire plastome (Molina et al., 2014). However, even among
68
      angiosperms that remain fully photosynthetic, there have been repeated accelerations in rates of
69
      plastid gene evolution (Jansen et al., 2007; Guisinger et al., 2008; Knox, 2014; Sloan et al., 2014;
70
      Dugas et al., 2015; Nevill et al., 2019; Shrestha et al., 2019). These accelerations in angiosperms
71
      that retain a photosynthetic lifestyle can be highly gene-specific (Magee et al., 2010) and are
72
      often most pronounced in non-photosynthetic genes, such as those that encode ribosomal
73
      proteins, RNA polymerase subunits, the plastid caseinolytic protease (Clp) subunit ClpP1, the
74
      acetyl-CoA carboxylase (ACCase) subunit AccD, and the essential chloroplast factors Ycf1 and
75
      Ycf2 (Guisinger et al., 2008; Sloan et al., 2014; Park et al., 2017; Shrestha et al., 2019).
      Accelerated protein sequence evolution has frequently been accompanied by other forms of
76
77
      plastome instability, including structural rearrangements and gene duplication (Guisinger et al.,
78
      2011; Knox, 2014; Sloan et al., 2014; Shrestha et al., 2019), as well as accelerated mitochondrial
79
      genome evolution in some cases (Cho et al., 2004; Parkinson et al., 2005; Jansen et al., 2007;
```

Mower et al., 2007; Sloan et al., 2009; Park et al., 2017). Several explanations have been

proposed for the cause of these cases of rapid plastome evolution, but they largely remain a mystery (Guisinger et al., 2008; Park et al., 2017; Williams et al., 2019). Discovering the full suite of nuclear genes that repeatedly co-accelerate with plastid genes may advance our understanding of this angiosperm evolutionary puzzle.

Here, we develop an approach to apply genome-wide ERC analyses across diverse angiosperms to identify hundreds of nuclear genes that exhibit signatures of ERC with the plastome. This set of genes is highly enriched for known N-pt genes with functions in several pathways that appear to be centered around maintenance of plastid protein homeostasis (proteostasis). We also observe strong signatures of plastid-nuclear ERC for more than 30 non-plastid-targeted proteins, representing candidates for novel plastid-nuclear interactions. Together, our findings impact our understanding of the genome-wide landscape of plastid-nuclear interactions.

### Results

Genome-wide ERC analyses detect correlated evolution between the plastome and N-pt genes.

We sampled 20 angiosperm species to perform a genome-wide scan for plastid-nuclear ERC. Given that the signature of ERC relies on phylogenetic rate heterogeneity, we sampled species that are known to exhibit differences in evolutionary rate for at least some plastid genes, including seven representatives of accelerated lineages (Jansen et al., 2007; Guisinger et al., 2008; Knox, 2014; Sloan et al., 2014; Dugas et al., 2015; Nevill et al., 2019; Shrestha et al., 2019) and 13 species that exhibit the slow background rate of plastome evolution typical for most angiosperms (Fig.1; Table S1). We did not include parasitic species with accelerated plastome evolution, as these represent special cases of plastid evolution associated with loss of photosynthetic function (Wicke et al., 2016). Because our ERC analysis employs a root-to-tip strategy for measuring branch lengths (described below), we avoided sampling pairs of species that are closely related to each other in order to minimize pseudoreplication caused by shared internal branches (Felsenstein, 1985; Yan et al., 2019). We included *Amborella trichopoda* and *Liriodendron chinense* as outgroups. We chose to include two outgroups so gene families would

112 contain an outgroup sequence even if gene loss occurred in one of the two species, allowing us to 113 analyze a larger proportion of gene families. It should be noted that phylogenetic placement of 114 magnoliids (including Liriodendron) with regard to the ingroup (eudicots and monocots) has been a topic of debate (Soltis et al., 1999; Zanis et al., 2002; Hilu et al., 2003; Qiu et al., 2005, 115 116 2006). However, large-scale analysis of the plastid genome resolved *Liriodendron* as an 117 outgroup to a eudicot/monocot clade (Jansen et al., 2007). We partitioned the plastid-encoded 118 proteins into seven functional categories: AccD, ClpP1, MatK, photosynthesis, ribosomal 119 proteins, RNA polymerase, and Ycf1/Ycf2 (Fig. 1; Table S2). 120 121 We applied a custom phylogenomic analysis pipeline to nuclear genomes and transcriptomes 122 (Fig. 2). Our pipeline included steps designed to extract gene families sharing orthology in the 123 presence of gene duplication and loss. It yielded a filtered set of 7929 gene trees with an average 124 of 25.1 sequences per tree and 16.4 species per tree (Fig. S1). Our genome-wide scan for plastid-125 nuclear ERC was executed by testing all possible 55,503 pairwise correlations between trees (7 126 plastome trees x 7929 nuclear trees) based on normalized branch lengths to account for lineage-127 specific features that may affect rates across entire genomes (e.g., generation time) (Clark & 128 Aquadro, 2010). To directly compare trees that can differ in topology, gene duplication, and 129 species representation, we measured branch lengths for each species on each tree using a 'root-130 to-tip' approach (Yan et al., 2019), in which we averaged the cumulative branch length of the 131 path leading from the common ancestor of all monocots and eudicots to each tip (gene copy) for 132 each species (see Methods). 133 134 To illustrate the ERC principle, we highlight a case study from the plastid Clp complex, which is 135 composed of the plastid-encoded ClpP1 subunit and multiple N-pt subunits (Nishimura & van 136 Wijk, 2015). This complex represents an effective positive control in the context of a genome-137 wide scan because it was previously shown to exhibit strong ERC signals among subunits 138 (Rockenbach et al., 2016; Williams et al., 2019). The Clp complex core is composed of two 139 heptameric rings, the 'R-ring' and 'P-ring'. ClpP1 is part of the R-ring and interacts more closely 140 with the other subunits in this ring (ClpR subunits) than with the subunits of the P-ring (ClpP 141 subunits) (Nishimura & van Wijk, 2015). These core rings are also accompanied by a variety of 142 accessory proteins (ClpC, ClpD, ClpF, ClpS, and ClpT subunits), allowing us to compare ERC

143 results for N-pt genes with varying degrees of physical interaction. A mirrored tree diagram of 144 ClpP1 and ClpR1 illustrates that branch lengths from corresponding species on the two trees 145 exhibit strong ERC ( $R^2 = 0.94$ ; Fig. 3A-B). Extending this analysis to all nuclear genes, a 146 genome-wide distribution of ERC results for ClpP1 reveals that 11 of the 13 known Clp proteins 147 (85%) exhibit an uncorrected p-value of < 0.05. Further, all ClpR and ClpP subunits are present 148 among the strongest ERC hits (top 2% of all genes analyzed), and all but one maintain genome-149 wide significance after correcting for multiple tests (Fig. 3C). We also find a general pattern of 150 clustering of ERC values between ClpP1 and other Clp subunits that corresponds to the intimacy 151 of their known interactions; ClpR subunits display the strongest ERC, followed by ClpP 152 subunits, with the accessory Clp subunits showing the weakest signal. 153 154 ClpP1 exhibits some of the most dramatic rate accelerations among plastome partitions (Fig. 1). 155 Therefore, to assess how the magnitude of rate variation affected the statistical power of ERC, 156 we also performed case studies (Fig. S2) for the plastid ribosome, which exhibits intermediate 157 levels of acceleration (Fig. 1F), and the photosynthesis partition, which exhibits less dramatic 158 accelerations (Fig. 1E). As observed in the Clp case study, these analyses detected significant 159 ERC for much larger proportions of known interacting genes than would be expected by chance, 160 but the degree of this enrichment for ERC signals was weaker and appeared to reflect the 161 magnitude of rate variation in the corresponding plastome partition. For the plastid ribosome, 21 162 of the 34 nuclear genes (62%) had an uncorrected p-value < 0.05 for ERC with the plastome 163 ribosome partition, while 15 of 45 nuclear photosynthesis genes (33%) met this threshold for 164 ERC with the plastome photosynthesis partition (Fig. S2). Overall, ERC appears to be 165 sufficiently sensitive to detect functional plastid-nuclear interactions even with the background 166 of a genome-wide scan. 167 168 We performed ERC analyses in parallel for each of the seven plastome partition trees against 169 normalized branch lengths from the nuclear trees (Table S3). We found that N-pt genes are 170 highly significantly overrepresented in ERC hits for all plastome partitions, displaying roughly 171 two-fold enrichment (Fig. 4). We identified the subset of these genes that are known to directly 172 physically interact with plastid-encoded proteins based on the CyMIRA classification (Forsythe 173 et al., 2019) and observed an even higher degree of enrichment (approximately 4-fold to 8-fold

depending on the plastome partition). We also found correlations between plastome partitions and nuclear genes with mitochondrial function. Overall, mitochondrial-targeted (N-mt) proteins are significantly enriched among ERC hits for all plastome partitions except for RNA polymerase and photosynthesis, although the effect size (approximately 1.5-fold) was smaller than for N-pt genes. N-mt proteins involved in direct physical interactions with mitochondrial-encoded proteins showed an increased degree of enrichment compared to all N-mt proteins (approximately two-fold), which was significant for all partitions. Proteins with dual localization to both plastids and mitochondria displayed wider variance of enrichment with inconsistent significance, both of which may be related to the small sample size of this gene category. Finally, we found that genes annotated as localized to any parts of the cell other than the plastids or mitochondria are significantly depleted among ERC hits for all partitions (Fig. 4). These results indicate that correlated plastid-nuclear evolution is pervasive across the nuclear genomes and this signature is detectable by ERC.

Functions associated with plastid proteostasis are highly enriched in ERC hits

Gene Ontology (GO) analyses of the ERC hits showed that several categories associated with plastid and mitochondrial function were significantly enriched, while GO terms associated with other cellular compartments (e.g., 'Nuclear' and 'Endomembrane') were significantly depleted (Fig. 5). Combined with the targeting data presented above (Fig. 4), these results reinforce the power of ERC in detecting cytonuclear interactions. Further, many of the enriched GO terms are more specifically connected to regulation of plastid proteostasis (Fig. 5). For example, terms related to proteolytic activity (e.g. 'protein quality control', 'chloroplastic Clp complex', and 'peptidase activity') display some of the highest degree of enrichment (more than 8-fold in some cases). This signature is further supported by detection of multiple subunits related to FtsH metalloproteases (Table 1). Translational machinery is also prominent; we found enrichment for several related GO categories (e.g. 'translation', 'ribosome biogenesis', 'chloroplast rRNA processing'), and many individual genes that encode plastid ribosomal proteins or are involved in translation initiation/elongation (Table 1). The GO terms 'protein transmembrane transport' and 'protein localization to chloroplast' are also enriched, indicating genes involved in chloroplast protein import (Table 1). The above functions constitute key regulators of plastid proteostasis

205 (Kim et al., 2013; Dogra et al., 2019), pointing to a possible driver of plastid-nuclear 206 coevolution. 207 208 Interestingly, the only significantly enriched GO category that is not directly related to plastid or 209 mitochondrial-localized function was 'cytosolic ribosome', which also has a clear role in 210 translation. We found that each of the identified cytosolic ribosome gene families contained 211 multiple Arabidopsis paralogs, and we confirmed that these were bona fide cytosolic ribosomal 212 subunits rather than misannotations of plastid ribosomal subunits in the GO classification scheme 213 (Fig. S4). This result suggests that factors that impact the rate of evolution of plastid genes (and 214 N-pt interaction partners) may also impact cytosolic ribosomes, pointing to potential regulation 215 of plastid proteostasis via maintenance of cytonuclear stoichiometry (see Discussion). 216 217 ERC analyses identify candidates for novel plastid functions 218 219 As previously mentioned, the individual hits with the strongest signatures of ERC are dominated 220 by known N-pt or N-mt genes (76%; Table 1). These hits include eleven genes that have been 221 annotated as organelle-localized but designated as 'proteins of unknown function'. ERC for these 222 genes provides evidence that could help resolve their roles in plastids. In addition, we observed 223 31 genes (24%) that are not annotated as plastid or mitochondrial-localized by CyMIRA 224 (Forsythe et al., 2019) (Table 2). These are candidates for novel N-pt genes and may contribute 225 to some of the functions described in the previous section. We discuss some of the most 226 intriguing examples below, including potential novel plastid proteostasis regulators. In sum, our 227 results indicate the specific pathways that exhibit plastid-nuclear ERC and reveal novel N-pt 228 candidates, leading to new hypotheses to advance our understanding of the full scope of plastid-229 nuclear interactions and their impact on plant evolution. 230 231 232 **Discussion** 233 234 Genomic signatures of plastid-nuclear interactions can be detected with ERC in plants 235

ERC has revealed novel interactions in animals and fungi but, until now, has not been applied at broad phylogenetic scales in plants due to the prevalence of gene/genome duplication. We adapted existing techniques, initially developed with the stringent requirement of one-to-one orthology, to make them more tolerant of duplications, thus allowing us to analyze a substantial portion of plant nuclear genomes. Our pipeline (Fig. 2) included several features tailored to analyze plant genomes. For example, our orthologous subtree extraction procedure identified subtrees with reduced paralogy compared to input trees, shifting the distribution of trees closer to one-to-one orthologous relationships without substantial loss of data (Fig. S1). In addition, our iterative gene tree/species tree (GT/ST) reconciliation approach resolved topological disagreements when they lacked phylogenetic support, allowing us to minimize phylogenetic noise while retaining well-supported phylogenetic signature. The typical implementations of ERC assume every gene tree has the exact same sampling and topology (Clark & Aquadro, 2010; Clark et al., 2012; Findlay et al., 2014; Wolfe & Clark, 2015). However, this is rarely the case in plant datasets, which are prone to topological variation introduced by internal duplications, incomplete lineage sorting, and differential gene loss (Degnan & Rosenberg 2009; Leebens-Mack, Barker, Carpenter et al., 2019), making it infeasible to compare individual branches in a one-to-one fashion between gene trees and to apply model-based evaluation of correlation from joint likelihoods (Clark & Aquadro, 2010). This challenge prompted us to apply a root-to-tip approach to calculating branch lengths. A drawback of this approach is that it introduces pseudoreplication via sampling shared internal branches multiple times (Felsenstein, 1985; Yan et al., 2019). We minimized this effect with our taxon-sampling by avoiding closely related species and, thus, approximating a 'star-phylogeny' as closely as possible. Finally, when multiple paralogs were present in a gene tree, we averaged the branch lengths between all paralogs for a given species. This approach allowed us to accommodate localized duplication events within trees. Our results offer proof-of-principle that ERC can be successfully extended to plant genomes at phylogenetic scales spanning angiosperm diversity and likely further. While we focused on plastid-nuclear interactions, our results open the door to applying this method broadly to probe the entire plant interactome.

236

237

238

239

240

241

242

243

244

245

246

247

248

249

250

251

252

253

254

255

256

257

258

259

260

261

262

263

264

265

266

We used the plastid Clp, plastid ribosome, and photosynthetic enzyme complexes as case studies to assess the performance of ERC (Fig. 3 and Fig. S2). In all three cases, known interactors are

267 enriched among the ERC hits, demonstrating the power of ERC to detect functional interactions. 268 Each plastome partition also returned a number of ERC hits for genes that are not known 269 interactors. Given that ERC has been demonstrated between non-physically interacting but 270 cofunctional genes (Clark et al., 2012), these genes may represent putative novel interactors. 271 Indeed, the predominance of known N-pt proteins among these ERC hits indicates that ERC 272 selectively returns genes with plastid functions (Fig. 4 and Fig. 5), pointing to cofunctionality as 273 a driver of ERC. However, it is also possible that a subset of the putative novel interactors are the 274 result of noise rather than functional interaction. As such, there will be an obvious need for 275 experimental validation of any newly identified interactions of interest. 276 277 Despite some uncertainty regarding interpretation of false positives, known interactions in our 278 case studies do allow at least a rough assessment of the features that impact the power of ERC. 279 The plastome partition trees used for each of these case studies exhibit a range of rate 280 acceleration (Fig. 1), and this appears to roughly correlate with the predictive power of ERC, as 281 ClpP1, ribosomes, and photosynthesis returned significant ERC hits for 85%, 61%, and 33% of 282 known interactors, respectively. Further, unlike the Clp analysis, the strongest ERC hits for the 283 plastid ribosome and photosynthetic enzymes were not known interactors. Therefore, the 284 strength of signal may decline for plastome partitions that are more conserved in sequence and 285 exhibit less rate variation across taxa. 286 287 Another factor that may limit the power of ERC is the extent to which functional rate covariation 288 is concentrated on individual residues or individual proteins. This factor comes in to play at two 289 levels in our analysis. Our nuclear gene trees are inferred from alignments of full protein 290 sequences (trimmed to remove poorly aligned regions), meaning that branch length estimates are 291 averaged across the full length of proteins. If rate covariation in concentrated on a small number 292 of residues (Madaoui & Guerois, 2008; Ovchinnikov et al., 2014), this averaging process could 293 result in dilution of the true signal. Further, our strategy of concatenating multiple plastid genes 294 for some plastome partitions (Table S2), holds similar risks of diluting or mixing signals. On the 295 other hand, an advantage of averaging across full-protein and concatenated alignments is that 296 including more sequence data in an alignment could amplify signatures of functional covariation 297 that are widespread but subtle. Further, combining individual sites into full-protein alignments

and groups of known cofunctional plastid proteins into a concatenated alignment dramatically reduces the dimensionality of our pair-wise ERC comparisons, which is critical to scaling analyses to the whole genome. We reasoned that the advantages of using full-protein alignments and concatenating genes together outweigh the risks of signal dilution, especially given that there is evidence that ERC signature is often distributed along primary protein sequence, rather than being concentrated on individual residues (Clark et al., 2012). However, future analyses aimed at pinpointing the specific genes and residues that drive the broad signatures of ERC that we detect could provide further insight into the mechanisms of plastid-nuclear coevolution.

306

307

308

309

310

311

312

313

314

315

316

317

318

319

320

321

322

323

324

325

326

327

328

298

299

300

301

302

303

304

305

Taken together, our results illustrate the impacts of plastid-nuclear interactions on evolutionary rates at a genome-wide scale. However, it is important to consider the correlative nature of ERC and the fact that detected effects do not always imply direct functional interactions. For example, we observe significant enrichment of N-mt proteins among our ERC hits (albeit a much weaker signal than for N-pt genes; Fig. 4 and Table 1). Given that our ERC searches were seeded with plastome partitions, it is tempting to interpret these signals as evidence for cofunctionality or crosstalk between mitochondria and plastids. Although such factors may contribute to the observed N-mt signal, the rates of evolution of the plastome and mitochondrial genome are known to be partially correlated with each other. Lineages such as *Plantago*, *Silene*, and Geraniaceae that exhibit rapid rates of plastome evolution in our sample (Fig. 1) also have unusually rapidly evolving mitochondrial genomes (Cho et al., 2004; Parkinson et al., 2005; Jansen et al., 2007; Mower et al., 2007; Sloan et al., 2009; Seongjun Park et al., 2017). As such, we would expect overlap between ERC hits from the two genomes even in the absence of cofunctionality between the mitochondria and plastids. Similarly, our plastome partitions do not evolve entirely independently of each other. Although the magnitudes of rate acceleration can vary greatly among genes (Fig. 1; (Guisinger et al., 2008; Sloan et al., 2014; Seongjun Park et al., 2017; Shrestha et al., 2019)), we observe significant ERC between all pairs of our plastome partition trees (Table S4), limiting our ability to distinguish specific signatures of ERC for individual partitions. Consistent with this, we found overlap between the hits identified for each partition (Fig. S3A-B). Multiple regression analyses provided some assistance in identifying the partitions making the strongest contributions to plastid-nuclear ERC (Fig. S3C-D, Tables 1 and 2), but further investigation will be needed to tease apart the effects of correlated rates of

evolution within and between cytoplasmic genomes in order to pinpoint the loci responsible for ERC with nuclear genes.

331332

333

334

338

339

340

341

342

343

344

345

346

347

348

349

350

351

352

353

354

355

356

357

358

329

330

Networks of cofunctional proteins are connected via their involvement in plastid proteostasis

ERC analyses point to plastid proteases, ribosomal proteins (subunits and binding/maturation

factors), translation initiation/elongation factors, and proteins involved in protein import into the plastids (Fig. 4, Table 1), all of which contribute to maintenance of protein quality control, proteostasis, and the unfolded protein response (Kim et al., 2013; Dogra et al., 2019; Heinemann

et al., 2020) (Fig. S5). Proteases exhibit some of the most striking signatures of ERC. In addition to Clp subunits, we observed strong ERC for FtsH7, FtsH9 and FtsH11. These proteins are

thought to form two separate protease complexes, both of which localize to the plastid envelope

(Ferro et al., 2003, 2010; Wagner et al., 2012). Interaction partners and substrates have been

identified for FtsH11 (Adam et al., 2019), but very little is known about the function of the

FtsH7/9 complex. These FtsH protease subunits do not appear to form a complex with any

plastid-encoded protein, making them an example of correlated plastid-nuclear evolution in the

absence of direct physical interaction. It is somewhat surprising that we did not observe

significant ERC for other members of the gene family that comprise the thylakoid FtsH protease

(FtsH1/2/5/8) considering that Clp mutants are suppressors of variegation phenotypes in

thylakoid FtsH mutants (Park & Rodermel, 2004; Yu et al., 2008). However, our results may be

consistent with the prior observation that expression of thylakoid FtsH subunits are unaffected by

Clp mutants, suggesting a lack of reciprocity in the interactions between Clp and the thylakoid

FtsH protease (Kim et al., 2013). On the other hand, we do observe strong ERC for additional

members of the FtsH family, FtsH12 and FtsHi5, which form part of a complex that facilitates

protein import across the inner membrane of the plastid, acting as an ATPase motor rather than a

protease (Kikuchi et al., 2018). Plastid-nuclear ERC for this complex may result from the fact

that it also contains plastid-encoded Ycf2 (another FtsH paralog) (Kikuchi et al., 2018). These

and other genes involved in protein import (most notably, TIC110) (Table 1) point to the strong

signature of plastid-nuclear evolution exhibited by import machinery, again highlighting the

prominence of proteostasis pathways in our ERC hits.

We observed ERC for several plastid ribosomal subunits and other genes involved in plastid translation (Table 1). For example, SVR7 is a pentatricopeptide repeat (PPR) protein that is involved in plastid rRNA processing, which (like Clp subunits) can act as a suppressor of thylakoid FtsH mutant variegation (Liu et al., 2010), again pointing to functional connections between plastid translation and other proteostasis pathways. However, perhaps our most surprising piece of evidence for the role of translation in plastid-nuclear ERC is the association between ClpP1 and protein subunits of the cytosolic ribosome (Fig. 4 and Fig. S4). While ERC has been previously detected among cytonuclear subunits in plastid and mitochondrial ribosomes (Sloan et al., 2014; Weng et al., 2016), the cytosolic ribosomes themselves have never been demonstrated to exhibit ERC with the mitogenome or plastome. Most of the plastid proteome is synthesized in the cytosol, meaning the levels of N-pt and plastid-encoded proteins must be regulated to achieve stoichiometric balance for cytonuclear complexes (Colombo et al., 2016). In mitochondria, this balance is achieved through coordination of cytosolic and mitochondrial translation (Houtkooper et al., 2013; Couvillion et al., 2016). Recent evidence suggests that changes in cytosolic translation may have strong genetic interactions with plastid proteostasis machinery. Specifically, mutation of a cytosolic ribosome subunit was shown to enhance variegation phenotypes in thylakoid FtsH mutants (Wang et al., 2018). Given that disruption of plastid translation can suppress these same phenotypes (Yu et al., 2008; Liu et al., 2010; Zheng et al., 2016), it appears that ribosomes in both compartments play a key role in maintenance of plastid-nuclear stoichiometric balance. Additionally, we observe strong ERC for a putative tRNA pseudouridine synthase (AT1G09800) that shows no evidence of plastid or mitochondrial targeting (Table 2), meaning it likely modifies cytosolic tRNAs, again consistent with cytosolic translation being subject to plastid-nuclear selection. These results suggest that the effects of perturbation in plastid proteostasis may extend to cytosolic ribosomes, supporting a level of cofunction-mediated ERC that spans cellular compartments. Genes involved in various aspects of proteostasis appear to have been subject to accelerated protein evolution in independent angiosperm lineages. We propose that proteostasis systems have been perturbed in these lineages, causing shifts in selection that simultaneously affected numerous functionally related genes. Although the evolutionary events that may have led to

these changes are unclear, one possible explanation could be related to the constant

360

361

362

363

364

365

366

367

368

369

370

371

372

373

374

375

376

377

378

379

380

381

382

383

384

385

386

387

388

389

stoichiometric pressure plants experience in the face of nuclear gene/genome duplication (Birchler & Veitia, 2012; Sharbrough et al., 2017). Similarly, the susceptibility of plastomes to instability and rearrangements in certain angiosperm lineages (Jansen et al., 2007) could provide an initial trigger that elicits a series of coevolutionary responses. It has also been hypothesized that antagonistic interactions between the nucleus and selfish genetic elements in the plastids could drive accelerated rates of evolution (Rockenbach et al., 2016; Sobanski et al., 2019). Finally, perturbations could be prompted by changes in abiotic or biotic stress, as many of the pathways that contribute to proteostasis are stress-responsive (e.g., the unfolded protein response to photooxidative stress) (Dogra et al., 2019; Heinemann et al., 2020). The cause of these perturbations may differ by lineage and disentangling them could reveal a critical driver of plant genome evolution. Regardless of the mechanisms, it is striking that the ripple effects are apparent across disparate pathways and cellular compartments and can be detected against the background of the entire genome in a large swath of plant diversity.

ERC points to novel plastid-nuclear interactions

Decades of proteomics research have led to the identification of more than 2,400 plastid-localized proteins in *Arabidopsis* (http://ppdb.tc.cornell.edu; http://cymira.colostate.edu/). Yet, these proteins may only represent about 70% of the plastid proteome (Millar et al., 2006; van Wijk & Baginsky, 2011; Christian et al., 2020). Large-scale plastid proteomic surveys are limited by ascertainment bias associated with protein expression level, tissue- and condition-specificity of expression/plastid-localization, and biochemical properties that impact mass spectrometry (van Wijk & Baginsky, 2011). ERC offers an alternative line of evidence for plastid function/localization that is complementary to biochemical approaches and may not share the same biases. Our analyses returned several proteins that lack plastid-targeting annotations (Table 2) and represent candidates for novel N-pt proteins. For example, two of our strongest non-plastid-localized hits are annotated as RNA-binding (AT5G59860) and GPI-anchored adhesin-like (AT1G16750) proteins based on *in silico* predicted domains but are, otherwise, lacking in functional information. The signature of plastid-nuclear ERC that we observe for the genes in Table 2 suggests they have experienced correlated changes selection associated with accelerated plastome evolution. A natural hypothesis is that these are cryptic N-pt proteins that

have evaded biochemical identification and curation in CyMIRA and its underlying databases (Forsythe et al., 2019). However, an alternative explanation is that they contribute to plastid function without localizing to plastids, similar to our hypothesis for cytosolic ribosomes and the pseudouridine synthase described above. A third possibility is that the proteins are plastid-localized in many plants but not in *Arabidopsis*, which is possible given the apparent lability of plastid-targeting across plants (Christian et al., 2020; Costello et al., 2020). While each of these explanations come with their own functional and evolutionary implications, future work to disentangle these alternative hypotheses will undoubtably advance our understanding of the full repertoire of plastid-nuclear interactions.

Methods

Obtaining and processing sequence data

Our analysis was conducted on publicly available genomes and transcriptomes. We obtained the full set of 20 proteomes from several sources (Table S1) and processed fasta files to add standardized sequence identifiers. For genome-based datasets that contained multiple splice variants per gene, we used only the first gene model (i.e. gene model ending in .1) and removed the rest to avoid falsely defining splice variants as paralogs in gene family clustering.

Plastome gene datasets were extracted from GenBank files (see Table S1) using a custom BioPerl script and manually curated to deal with missing annotations and inconsistent naming conventions. The corresponding protein sequences were either analyzed individually (ClpP1, AccD, and MatK) or concatenated from multiple plastid genes that are part of a common plastid complex and/or pathway (photosynthesis, ribosomes, RNA polymerase, and Ycf1/Ycf2) (Table S2). The plastome sampling matched the nuclear proteome samples described above except that no plastome sequence was available for *Acacia aulacocarpa*, so we used the *Acacia ligulata* plastome in its place. The *accD* gene is missing from the plastome of *Oryza sativa* and *Lobelia siphilitica*, and *ycf1* and *ycf2* are missing from *Oryza sativa* and *Geranium maderense*. These species were omitted from the alignments and trees for AccD and Ycf1/Ycf2. Amino acid alignments based on plastome partitions were used to estimate branch lengths on a constraint tree

453 with a topology based on Angiosperm Phylogeny Website 454 (http://www.mobot.org/MOBOT/research/APweb) (Fig. 1). 455 456 Gene family clustering, sequence alignment, and phylogenetic inference 457 458 We clustered homologous gene families using Orthofinder (v2.2.6) (Emms & Kelly, 2015) and 459 performed multiple sequence alignment using the L-INS-i algorithm in MAFFT (v7.407) (Katoh 460 & Standley, 2013). We used RAxML (v8.2.12) (Stamatakis, 2014) to infer maximum likelihood 461 trees with 100 bootstrap replicates. Tree inference was performed using the command below for 462 each gene. The -m argument indicates the model used (gamma distributed rate heterogeneity, 463 empirical amino-acid frequencies, and the LG substitution model). The -p argument provides a 464 seed for parsimony search. The -x argument provides a seed for rapid bootstrapping. The -# 465 argument indicates the number of bootstrap replicates. The -f a argument implements rapid 466 bootstrap analyses and best scoring tree search. The -T argument indicates the number of threads 467 used for parallel computing. 468 469 raxmlHPC-PTHREADS-SSE3 -s <input file name> -n <output file name> -m 470 PROTGAMMALGF -p 12345 -x 12345 -# 100 -f a -T 24 471 472 For the step in which we optimized branch lengths on a constraint tree (see below), we used the 473 following command, with -f e indicating parameter and branch-length optimization. 474 475 raxmlHPC-PTHREADS-SSE3 -s <input file name> -n <output file name> -t <name of constraint 476 tree file> -m PROTGAMMALGF -p 12345 -T 24 -f e 477 478 Subtree extraction and quality control pipeline 479 480 ERC analyses are sensitive to false inferences of orthology. Particularly, treating cryptic out-481 paralogs as orthologs can alter branch length estimates (Smith & Hahn, 2020). While 482 Orthofinder clusters sequences that share homology, these clusters do not always represent 483 groups that share strict orthology. ERC analyses are also sensitive in poorly aligned sequences,

which can result in long outlier branches on trees. To address these inherent challenges to genome-scale phylogenetic analyses, we built a pipeline to process nuclear gene trees and retain the portions of alignments and trees least likely to be affected by biasing factors. Our pipeline enlists several existing programs. In this section we provide a summary of the steps in the pipeline and point the reader to subsequent sections for details on our application of individual components of the pipeline.

490

491

492

493

494

495

496

497

498

499

500

501

502

503

504

505

506

507

508

484

485

486

487

488

489

(Step 1) Starting with the full gene trees we performed GT/ST reconciliation in order to root the tree, rearrange poorly supported portions of the tree to conform with the species tree, and infer nodes in the tree that represent gene duplication rather than speciation. (Step 2) We used duplication information from step 1 to extract subtrees representing orthology groups. (Step 3) We performed a second round of sequence alignment (using MAFTT as above) to generate alignments that contain only the sequences in subtrees. (Step 4) We trimmed these alignments to remove poorly aligned regions using GBLOCKS. We filtered out any alignments with a length of less that 50 amino acids as well any alignments for which GBLOCKS trimming resulted in the removal of an entire sequence from the alignment. (Step 5) We inferred a new phylogeny for each subtree from the trimmed alignment using RAxML as above and again applied GT/ST reconciliation to the subtree trees to rearrange poorly supported nodes and root the tree. (Step 6) We used the reconciled versions of the gene trees (as constraint trees) and the trimmed version of the alignments to optimize final branch lengths for use in downstream ERC analyses. (Step 7) As a final means of quality control before performing ERC analyses, we assessed each tree to ask whether the ingroup forms a monophyletic clade in the branch-length-optimized tree. Those that were not monophyletic were pruned and rerooted in order to retain ingroup monophyly. We also filtered out trees with one very long outlier branch by removing any trees in which the longest branch is more than ten times the length of the second longest branch.

509

### GT/ST reconciliation

511

512

513

514

510

We used GT/ST reconciliation to reconstruct the history of gene duplication for each gene tree using Notung (v2.9) (Vernot et al., 2008; Stolzer et al., 2012). Briefly, Notung compares the topology of a gene tree inferred from an individual gene to the topology of a user-input species

515 tree. We used the topology of the plastome trees described above as our species tree. 516 Incongruencies between the gene tree and species tree are taken to be the result of historical gene 517 duplication occurring at specific nodes of the tree. Notung uses a parsimony framework to reconcile these incongruences by inferring duplication and loss events along the gene tree to 518 519 yield the most parsimonious series of duplication and loss events for each gene tree. Notung can 520 also apply this logic to root unrooted gene trees by the most parsimonious root. Since topological 521 incongruence is the signature by which Notung infers duplication events, inferences are sensitive 522 to phylogenetic error, evidenced by branches with low bootstrap support. To avoid false 523 inference of duplication from weakly supported branches, we made use of Notung's option to 524 only infer duplication that is supported by branches with bootstrap support of at least 80 percent. 525 526 We performed the rearranging step for each gene tree on the command line with the following 527 command: 528 529 java -jar Notung-2.9.jar <path to gene tree file> -s <path to species tree file> --rearrange --530 threshold 80 --treeoutput nhx --nolosses --speciestag prefix --edgeweights name --outputdir 531 <output directory> 532 533 We performed the rooting step for each gene tree with the following command: 534 535 java -jar Notung-2.9.jar <path to rearranged gene tree file> -s <path to species tree file> --root --536 treeoutput nhx --nolosses --speciestag prefix --edgeweights name --outputdir <output directory> 537 538 In both of the above commands, --treeoutput nhx indicates trees to be output in the newick 539 extended format, which allows for the retention of duplication information. --nolosses indicates 540 that loss information is omitted from the output file (but still included in the reconciliation 541 process). --speciestag and --edgeweights instructs Notung where to find relevant information in 542 the input file. 543 544 Orthologous subtree extraction

We used duplication information from Notung to extract portions of gene trees (i.e. subtrees) in which the taxa share orthology relationships to each other (as opposed to paralogy). We required that these subtrees contain at least one eudicot, one monocot, and one outgroup sequence (Amborella trichopoda or Liriodendron chinense). We required that at least ten species be represented in each subtree and the eudicot and monocot taxa in the subtree (i.e. the ingroup) form a monophyletic clade. To extract subtrees that fulfill these criteria, for each gene tree we started by iteratively splitting the tree at each node indicated as a duplication node by Notung and retaining the two daughter trees from the splits. Daughter trees were assessed independently and those that fulfilled the above criteria were retained, meaning that multiple subtrees were retained from an initial gene tree in some cases. The final subtrees retained after this process were non-overlapping subtrees containing at least ten taxa representing eudicots, monocots, and at least one outgroup with eudicots and monocots forming a monophyletic clade.

Multiple sequence alignment trimming with GBLOCKS

We used GBLOCKS (v0.91b) (Castresana, 2000) to trim poorly aligned regions of our alignments using the below command, with -b4 indicating the minimum length of the retained block, -b5=h indicating that gaps are allowed in up to half of the total species, and -b2 indicating the minimum number of sequences for a flank position.

Gblocks <aln directory> <aln file name> -b5=h -b4=5 -b2=<half the total number of sequences>

Rerooting to retain ingroup monophyly following subtree phylogenetic inference

We realigned and inferred a new phylogeny for subtrees using the same methodology described above. In some cases, these new trees no longer placed eudicots and monocots (i.e. the ingroup) as a monophyletic group, which is a requirement of our downstream ERC analyses. This problem arose in trees in which there were multiple sequences from outgroup species and one or more of these taxa was nested within the ingroup causing the ingroup to be polyphyletic. For these trees, we identified the offending outgroup branches and pruned them from the tree. If *Amborella trichopoda* remained following pruning, we rooted on a branch leading to that species, choosing

577 one at random if there were multiple Amborella trichopoda sequences. If no Amborella 578 trichopoda branches remained, we rooted on Liriodendron chinense in a similar fashion. 579 580 ERC analysis 581 582 Branch lengths for ERC analyses were obtained from rooted branch-length-optimized gene trees. 583 The branch lengths for these trees were calculated with an LG substitution model, empirical 584 amino-acid frequencies, and gamma-distributed rate heterogeneity across sites (see RAxML 585 command above). We used a root-to-tip method that measures the collective lengths of the path 586 of branches from each ingroup tip to the node representing the most recent common ancestor of 587 all ingroup tips, allowing for phylogeny-aware measurement of the amino acid substitutions in 588 each lineage. We obtained these root-to-tip branch length measurements for all ingroup species 589 for each gene tree using dist.nodes() command from the Ape package (Paradis et al., 2004) in R. 590 When multiple paralogs from a given species were present, the mean root-to-tip distance from all 591 paralogs was used. When species were absent from trees, branch lengths were indicated as 592 missing values for those species and excluded from ERC analysis for those genes. To account for 593 lineage-specific differences in whole genome rate of evolution, we normalized the branch length 594 for each species be dividing the value for each tree by the average branch length for that species 595 across all genes in our analysis. These normalized branch length values were used for pairwise 596 ERC comparisons. 597 598 We compared each of the seven plastome partition trees against all nuclear trees. Each pairwise 599 comparison comprised a correlation analysis of the branch lengths for each species in the plastid 600 tree versus the branch lengths for the same species in the nuclear gene tree (see Fig. 3 for visual 601 depiction). For each pairwise comparison we calculated Pearson and Spearman correlation 602 coefficients. Because there is no clear biological expectation for significant inverse relationships 603 in ERC, we only considered genes with positive correlations (slope > 0) in downstream analyses. 604 We adjusted p-values for multiple comparisons using the false discovery rate (FDR) method 605 implemented with the *p.adjust()* function in *R*. 606

CyMIRA and Gene Ontology functional enrichment analyses

608 609 In order to perform functional enrichment analyses, we needed a threshold to separate our 'hits' 610 from our background genes. We chose to make use of p-values from both Pearson correlation 611 and Spearman correlation as metrics because Pearson gains power from large branch lengths, 612 potentially expected under true evolutionary co-acceleration, and Spearman is less sensitive to 613 outlier branches. Any gene with a Pearson p-value  $\leq 0.05$  and a Spearman p-value  $\leq 0.1$  was 614 designated as a 'hit'. Our goal here was to identify the tail of the distribution for the sake of 615 functional enrichment analysis. A more stringent threshold was applied when assessing the 616 significance of individual hits (Table 1 and 2). 617 618 We used the *Arabidopsis* sequence identifiers present within gene families to probe functional 619 enrichment of significant hits based on localization/interaction annotations from CyMIRA and 620 functional annotations from Gene Ontology. We used the 7929 genes in our filtered dataset as 621 the background (rather than using the full Arabidopsis genome). For gene families that contained 622 multiple Arabidopsis paralogs, we selected a single Arabidopsis paralog at random to represent 623 the family. Families that did not contain any Arabidopsis sequences were omitted from this 624 portion of the analysis. Fold enrichment was calculated as number of observed hits in a category 625 divided by the number of expected hits in a category, where the expected is the proportion of the 626 background in a category multiplied by the number of hits. The localization/interaction 627 enrichment analyses were performed in R. Gene Ontology enrichment analyses was performed 628 using the *PANTHER* web-based tool (http://geneontology.org/) (database release from 10-08-629 2019). Significance of enrichment was assessed with Fisher's Exact Test with an FDR correction 630 for multiple comparisons. 631 632 *Identification of genes displaying strong signatures of ERC.* 633 634 To identify individual genes displaying the strongest signatures of plastid-nuclear ERC, we 635 applied more stringent criteria that considered Pearson and Spearman correlation p-values in 636 their raw and FDR-corrected forms. Our criteria for labeling a gene as a strong hit is that either 637 the adjusted Pearson p-value or the adjusted Spearman p-value (or both) must be  $\leq 0.05$ .

Additionally, for the genes in which only one of the two adjusted p-values was ≤0.05, we also

639 required that the raw Pearson and raw Spearman p-value both be ≤0.05. This approach allowed 640 us to incorporate information from both correlation coefficients and from FDR multiple test 641 correction while still retaining power to detect the strongest hits. Genes passing these criteria are 642 presented in Table 1 and 2. 643 644 Multiple regression analyses 645 To investigate the relative contributions of each plastome partition to the evolutionary rates of 646 647 each nuclear-encoded protein, we conducted a multiple regression analysis using branch lengths 648 from our constructed trees. Due to the lack of accD in Oryza sativa and Lobelia siphilitica and 649 the lack of *ycf1/ycf2* in *Oryza sativa* and *Geranium maderense*, we excluded branch lengths 650 those three species, which allowed us to include all seven plastome partitions. Each nuclear gene 651 was analyzed separately, where the y values were the normalized branch lengths for each species 652 for that particular gene and the x values were the normalized branch lengths for each plastome 653 partition for each species. Any additional missing data led to removal of the involved species. 654 Models were created using the lm() function in R with default parameters. 655 656 Data availability 657 Alignments and phylogenetic trees used in this analysis have been deposited at Dryad Digital 658 Repository and can be accessed at: https://doi.org/10.5061/dryad.7h44j0zs3 659 660 Code used to conduct this analysis is available at: 661 https://github.com/EvanForsythe/Plastid nuclear ERC 662 663 664 **Author contributions and acknowledgements** 665 E.S.F., A.M.W., and D.B.S. conceived this work and performed analyses. E.S.F. drafted this 666 manuscript with input from all authors. This work was supported by a National Science 667 Foundation (NSF) grant (MCB-1733227) and graduate fellowships from NSF (DGE-1321845) 668 and the National Institutes of Health (T32-GM132057). We thank M.P. Simmons and J.C. 669 Havird for helpful discussion.

# Figures:

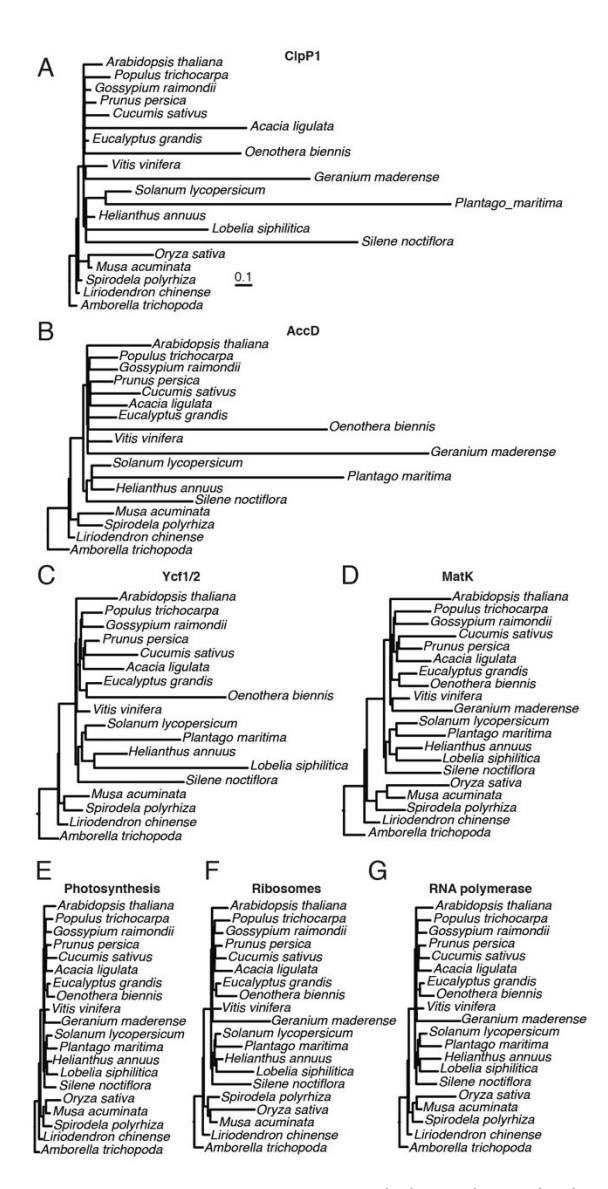


**Figure 1. Trees based on plastome partitions.** Branch length optimized trees inferred from amino acid sequence alignments for plastid genes partitioned into seven functional categories (described in Table S2). Branch lengths are shown on the same scale for all trees to highlight differences in rates of amino acid evolution among partitions. Each plastome partition tree was used for ERC analysis against all nuclear gene trees.

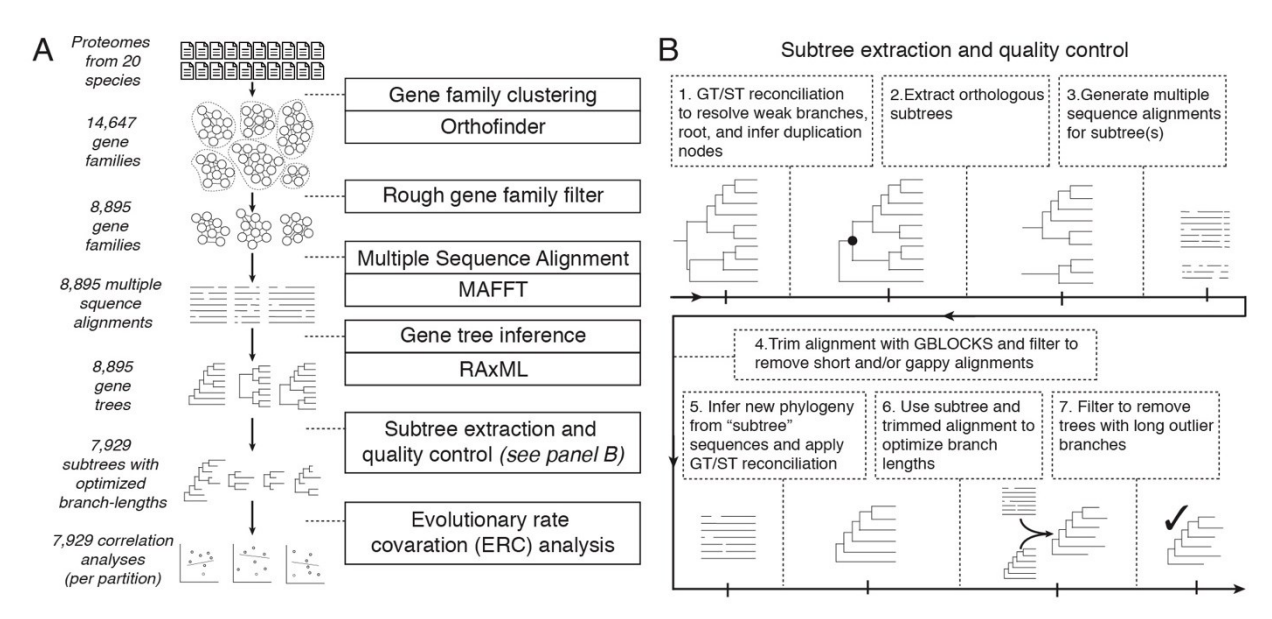


Figure 2. Phylogenomic pipeline used to identify and analyze nuclear gene families. (A) Flowchart depicting the steps leading up to ERC analyses. (B) Steps of the extraction and quality-control procedure.

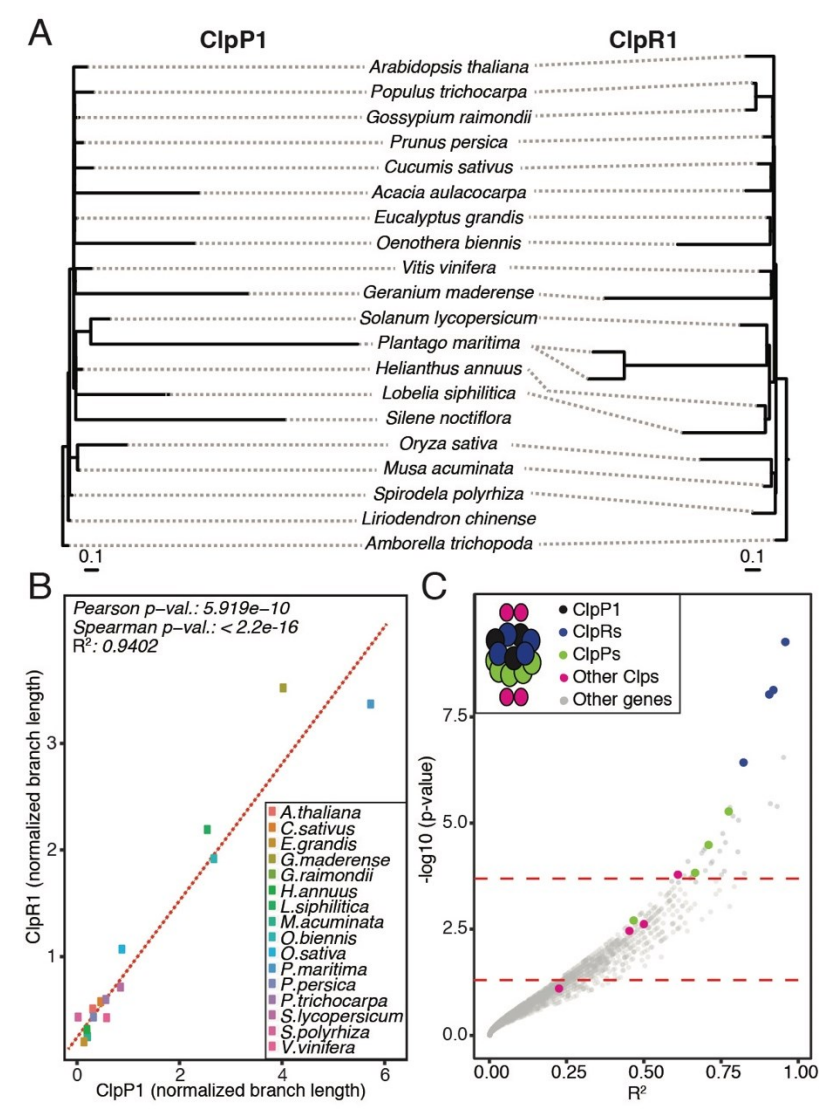


Figure 3. Case study of ERC between plastid-encoded ClpP1 and nuclear gene trees. (A) ClpP1 and ClpR1 gene trees shown mirrored to highlight correlation of branch lengths. (B) Linear regression quantifying correlation of evolutionary rates between ClpP1 and ClpR1. Points represent normalized branch lengths estimated from ClpP1 (x-axis) and ClpR1 (y-axis) gene trees. Dotted line indicates best fit trend line. (C) Results from ERC analyses of ClpP1 versus all nuclear genes. Each point represents p-value and R² values from a pairwise ERC analysis (Pearson correlation). ERC comparisons with negative slopes are not shown. Known Clp complex nuclear genes are colored by their placement in the Clp structure (depicted in the legend). Dotted lines indicate a raw p-value of 0.05 (bottom) and a genome-wide significance at an FDR-corrected p-value of 0.05 (top).

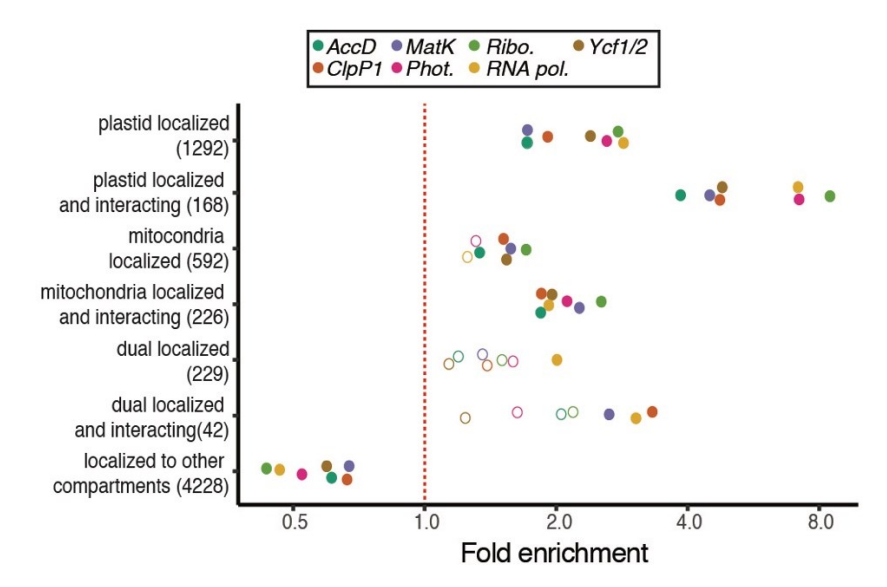
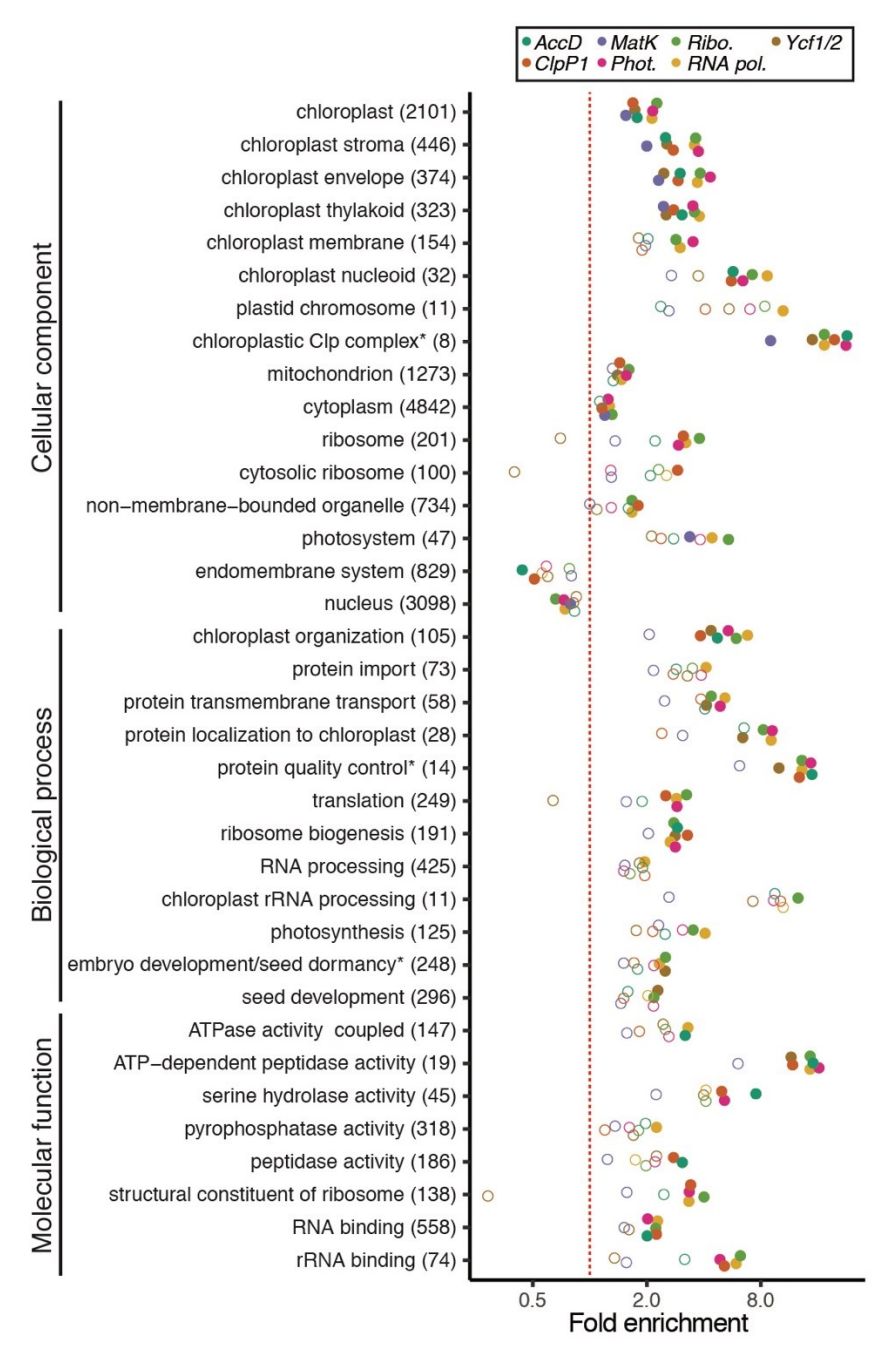
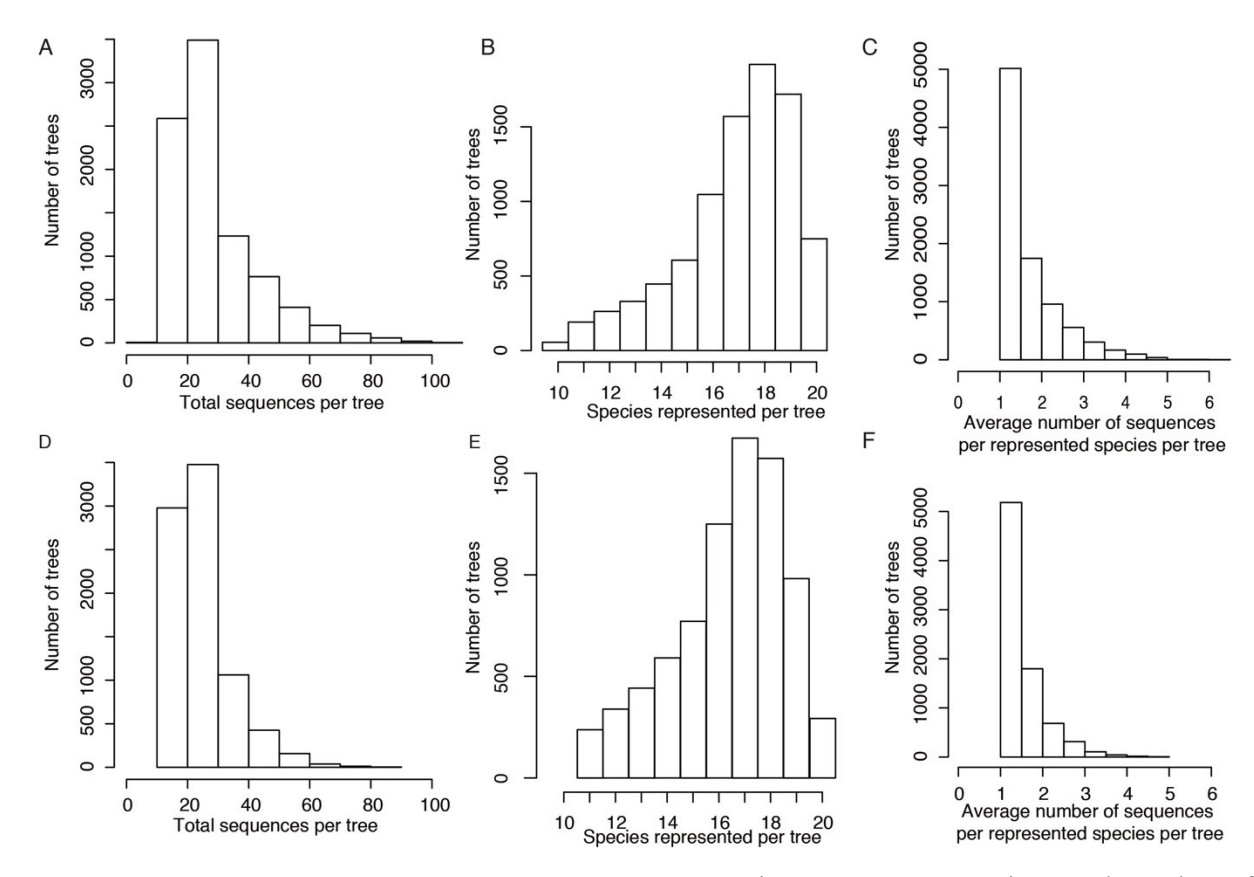


Figure 4. Subcellular localization and cytonuclear interactions of ERC hits. Genes exhibiting signatures of coevolution with plastome partitions were analyzed for their localization and interactions as classified by the CyMIRA database (Forsythe et al., 2019). Categories indicating 'interacting' refers to nuclear proteins predicted to directly physically interact with organelle-encoded proteins. The number of total genes in each category are indicated in parentheses. Statistical significance of enrichment/depletion (Fisher's exact test) is indicated by filled points (p < 0.05).



**Figure 5. Functional enrichment of ERC hits.** Gene Ontology (GO) functional enrichment analyses were performed for ERC hits from each of the plastome partitions. Categories with significant enrichment/depletion in at least one partition are shown. Categories are grouped by type of GO annotation (cellular component, biological process, molecular function). Some redundant or highly overlapping categories were removed (see Supplementary Data for full results). Asterisks indicate shortening of category name to fit figure dimensions. The number of total genes in each category are indicated in parentheses. Statistical significance of enrichment/depletion (Fisher's exact test) is indicated by filled points (p < 0.05). P-values were corrected for multiple tests using FDR.



**Figure S1. Taxon composition of trees and subtrees.** Histograms representing total number of sequences per tree (A and D), number of species represented per tree (B and E), and average number of sequences per represented species per tree (C and F). Distributions are shown for original trees before subtree extraction (see Methods) (A-C) as well as for final subtrees after orthologous subtree extraction (D-F). Supports Figure 1.

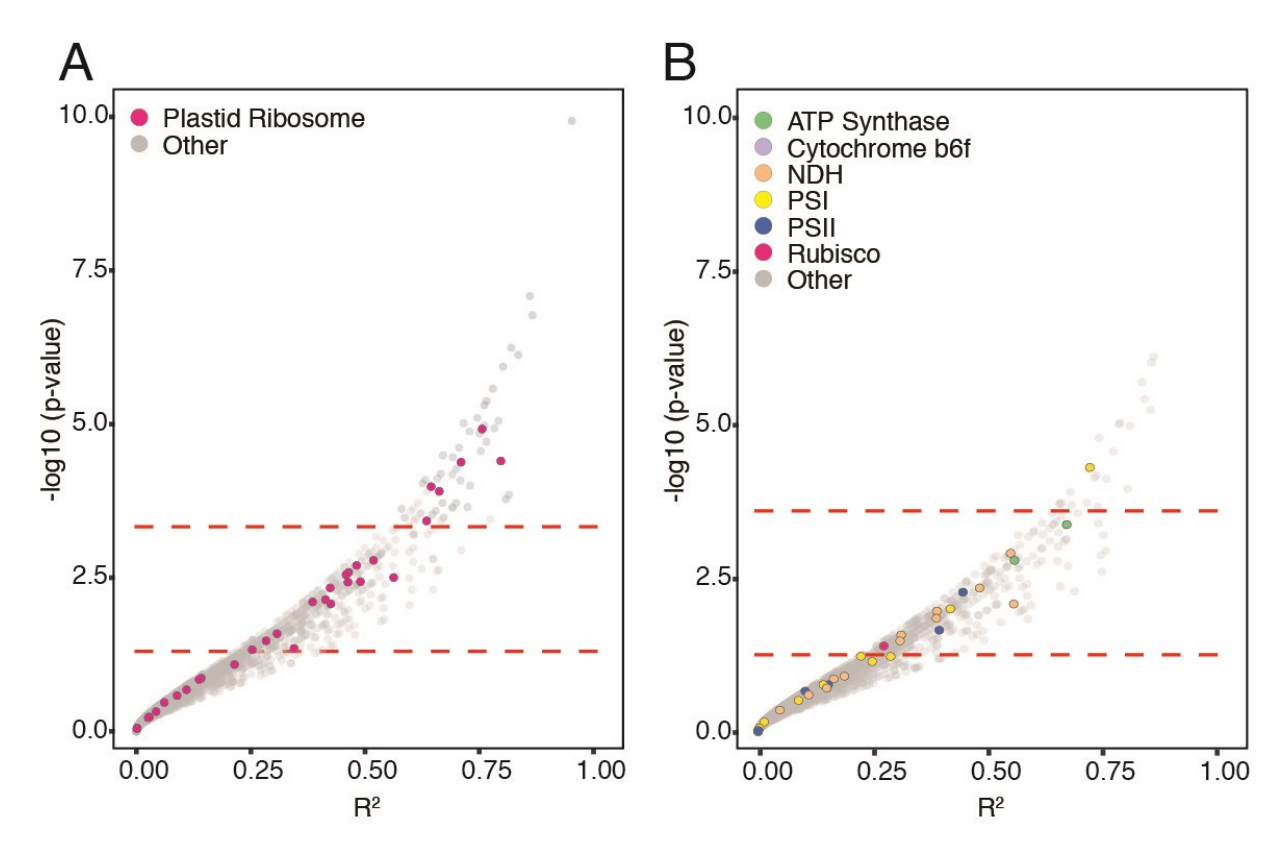


**Figure S2. ERC case studies for known plastid complexes.** Results from ERC analyses of the ribosome plastome partition (A) and photosynthesis plastome partition (B) versus all nuclear genes. Each point represents the p-value and R<sup>2</sup> value from a pairwise ERC analysis (Pearson correlation). ERC comparisons with negative slopes are not shown. Known plastid ribosome nuclear genes are colored in magenta (A), and known photosynthesis genes are colored according to complex (B). Dotted lines indicate a raw p-value of 0.05 (bottom) and a genomewide significance at an FDR-corrected p-value of 0.05 (top). Supports Figure 3.

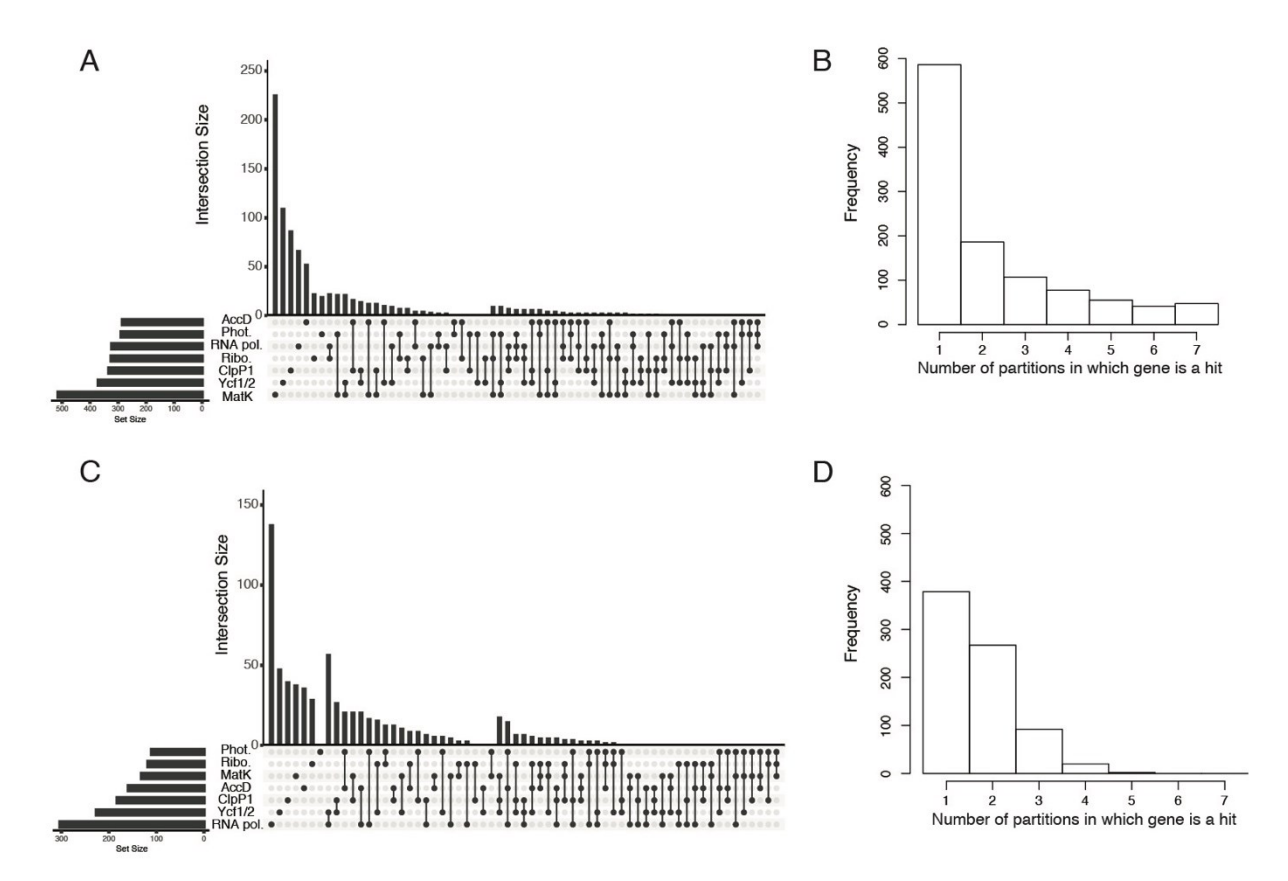


Figure S3. Plastome partition ERC result overlap and multiple regression analysis. (A-B) ERC hit overlap for the single-correlation analyses used in Figs. 4 and 5. (A) UpSet plot showing the overlap of ERC hits between partitions (Conway et al., 2017). Intersects of four or more partitions are not shown to save space. (B) Histogram showing the number of partitions in which each nuclear gene was a hit. (C-D) ERC hit overlap for the multiple regression analyses. (C) UpSet plot of the overlap of ERC hits between partitions. Intersects of four or more partitions are not shown. (D) Histogram of the number of partitions in which each nuclear gene was a hit. Supports Figures 4 and 5.

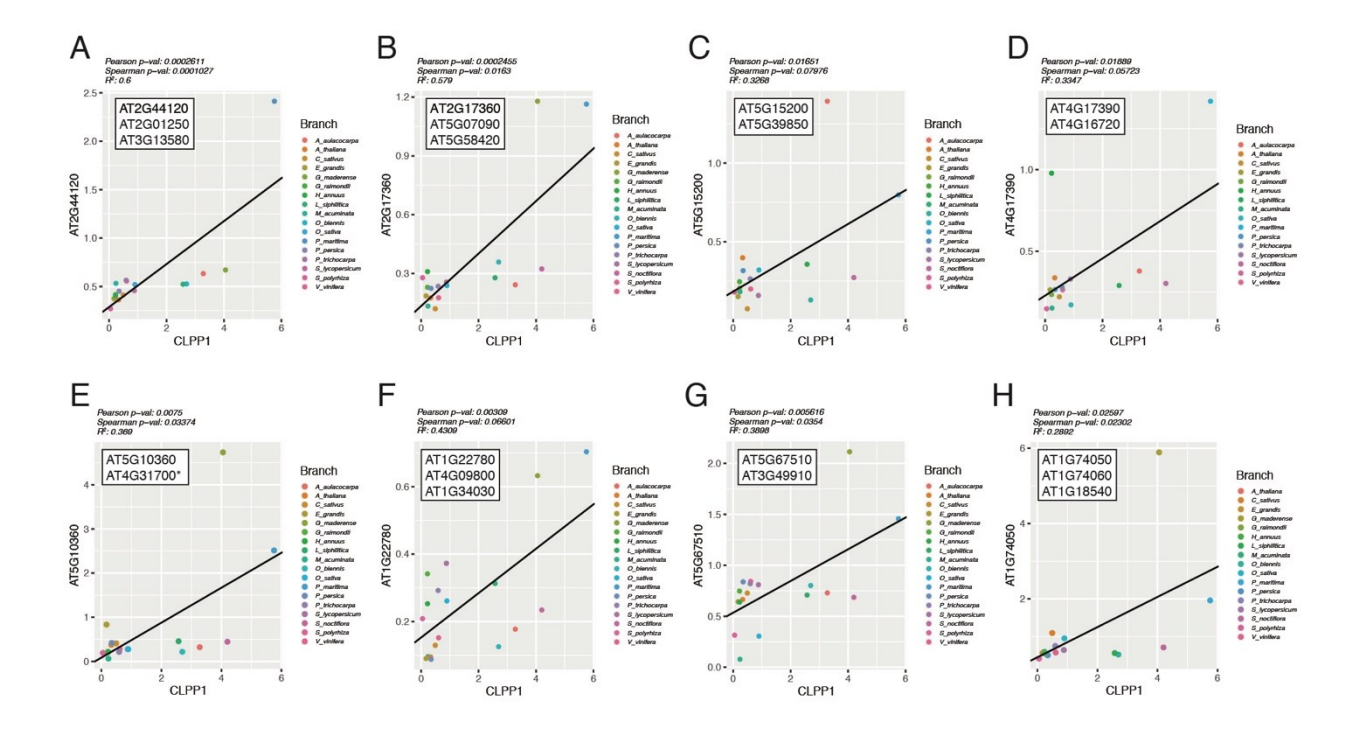


Figure S4. Cytosolic ribosome subunits found to have significant ERC with ClpP1. Correlation plots comparing normalized branch lengths from ClpP1 versus normalized branch lengths for cytosolic ribosome gene trees. All families contained multiple *Arabidopsis* paralogs. The y-axis labels indicate the AGI locus identifier for the randomly chosen paralog used for enrichment analyses. The white box insets list AGI locus identifiers for all Arabidopsis paralogs in each family. All loci shown were compared against previous datasets (Bonen & Calixte, 2005; Tiller et al., 2012; Sloan et al., 2014; Bieri et al., 2017; Boerema et al., 2018; Waltz et al., 2019) and found to be annotated as cytosolic ribosomes except for AT4G31700 (indicated with \*), which was not annotated as a ribosome subunit in the above studies but is annotated at a cytosolic ribosomal subunit elsewhere (Creff et al., 2010). Supports Figure 5.

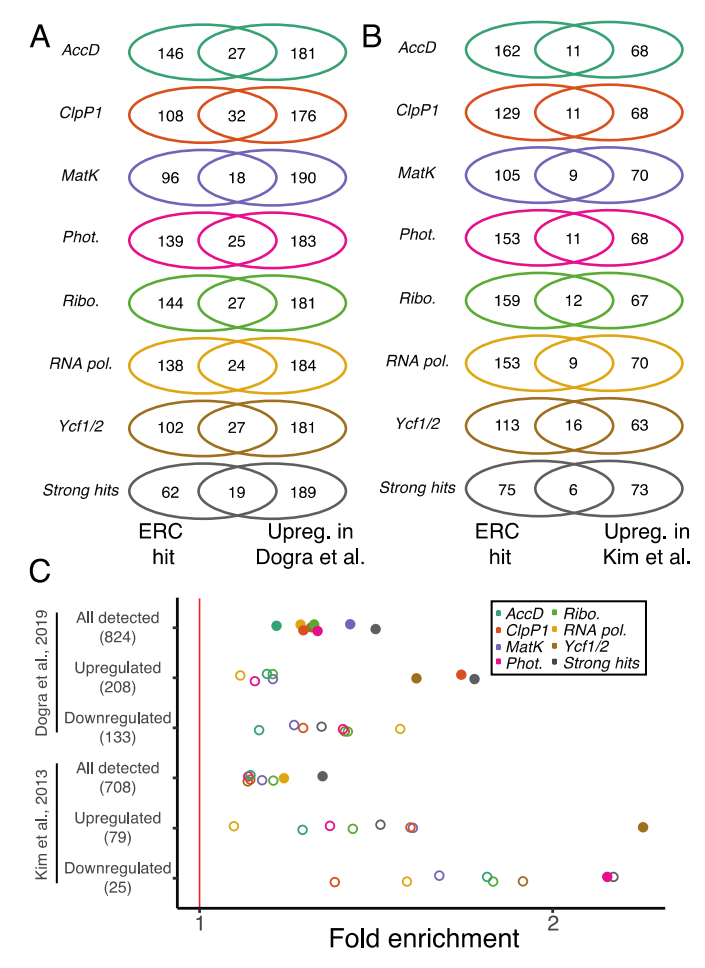


Figure S5. Comparison of ERC hits to genes with altered expression in proteostasis mutants. (A-B) Venn diagrams depicting overlap of ERC hits with upregulated chloroplast proteins from mutants for the metalloprotease subunit FtsH2 (Dogra et al., 2019) (A) and *ClpP3* (Kim et al., 2013) (B). (C) Enrichment analyses testing whether proteins detected with differential expression are enriched among ERC hits. For all panels, ERC hits were filtered to include only chloroplast-localized proteins according to CyMIRA (Forsythe et al., 2019). Supports Figure 5.

**Table 1: Organelle-localized strong ERC hits.** AGI locus identifiers are shown for nuclear genes with significant ERC with plastome partition(s). \* indicates significant ERC for the partition in multiple regression. \*\* indicates the shown partition was the only significant ERC under multiple regression. For genes that are hits in multiple plastome partitions, the slope, R<sup>2</sup>, and P-values for partition with the lowest Pearson P-value are reported. Shown here is a subset of the 99 total organelle-localized strong ERC hits. For full results see Supplementary Data.

	Plastome partition	AGI ID locus	Localiz ation	Gene symbol	TAIR description	Slope	R <sup>2</sup>	Adj. P (Pearson)	Adj. P (Spearman)	Mult. reg. P
on	Ribo., RNA pol., Phot., AccD, Ycf1/2, ClpP1	AT1G17220	СР	FUG1	Translation initiation factor 2, small GTP-binding protein	1.44	0.95	9.27E-07	3.49E-13	1.21E-01
Translation	Ribo., Phot.	AT1G62750	Dual	ATSCO1, ATSCO1/CPEF- G, SCO1	Translation elongation factor EFG/EF2 protein	2.61	0.78	2.35E-03	2.12E-01	5.03E-01
	AccD	AT5G67510	CP	NA	Translation protein SH3-like family protein	3.26	0.67	1.77E-02	7.08E-01	8.48E-02
	Ribo., RNA pol., Phot.	AT4G34730	CP	NA	ribosome-binding factor A family protein	0.50	0.84	8.52E-04		2.06E-02
Ribosomes	Ribo., ClpP1	AT2G33800	CP	NA	Ribosomal protein S5 family protein	0.41		5.31E-03	1.93E-01	5.04E-02
Son	MatK	AT5G02740	MT	NA	Ribosomal protein S24e family protein	0.33	0.81	7.67E-03	2.91E-13	1.33E-02
pos	AccD*	AT5G10360	CP	EMB3010, RPS6B	Ribosomal protein S6e			1.03E-02	6.91E-01	1.48E-02
<u>R</u>	Ribo., RNA pol.	AT3G44890	CP	RPL9	ribosomal protein L9	0.75	0.71	1.15E-02		9.37E-01
	Ribo.	AT5G40950	CP	RPL27	ribosomal protein large subunit 27	1.35	0.64	2.07E-02	7.26E-01	2.04E-01
	ClpP1	AT1G64880	MT	NA	Ribosomal protein S5 family protein		0.60	4.56E-02	8.90E-01	1.67E-01
	ClpP1*, AccD, Ribo., RNA pol., Phot.*	AT1G49970	СР	CLPR1, NCLPP5, SVR2	CLP protease proteolytic subunit 1	1.46	0.94	4.70E-06	2.49E-13	8.26E-06
	ClpP1*, AccD*, Ribo., Phot.	AT1G09130	Dual	NA	ATP-dependent caseinolytic (Clp) protease/crotonase family protein	1.30	0.89	2.68E-05	2.49E-13	5.82E-05
Clp	ClpP1*, AccD*	AT1G12410	CP	CLPR2, NCLPP2, CLP2	CLP protease proteolytic subunit 2	2.03	0.90	2.68E-05	5.44E-03	1.10E-03
	AccD, Ribo., RNA pol., Phot., ClpP1**, Ycf1/2	AT5G45390	СР	CLPP4, NCLPP4	CLP protease P4		0.87	4.64E-04	5.93E-01	3.17E-03
	ClpP1, AccD	AT4G17040	CP	CLPR4	CLP protease R subunit 4	2.21	0.81	6.08E-04	2.49E-13	4.45E-03
	AccD**, ClpP1	AT1G11750	CP	CLPP6	CLP protease proteolytic subunit 6		0.83	2.46E-03	6.00E-01	2.28E-03
	ClpP1, Ycf1/2, Ribo.	AT1G66670	CP	CLPP3, NCLPP3	CLP protease proteolytic subunit 3	2.62	0.76	4.52E-03	2.92E-01	6.46E-03
	AccD	AT5G58870	CP	ftsh9	FTSH protease 9	9.22	0.75	7.52E-03	6.96E-01	1.37E-02
FtsH	Ribo., ClpP1*, AccD, RNA pol., Phot.	AT5G53170	Dual	FTSH11	FTSH protease 11	1.47	0.76	3.27E-03	3.16E-01	1.05E-03
	RNA pol., Ribo.**, Phot.	AT4G16390	CP	SVR7	pentatricopeptide (PPR) repeat-containing protein	0.49	0.92	3.34E-05	4.50E-02	5.77E-04
	Ribo., Phot., RNA pol., AccD, Ycf1/2	AT5G66470	CP	NA	RNA binding; GTP binding	1.58	0.82	7.60E-04	2.47E-02	1.44E-01
ding	AccD, Ycf1/2, Phot.	AT4G31010	MT	NA	RNA-binding CRS1 / YhbY (CRM) domain-containing protein	8.39	0.87	9.07E-04	6.30E-01	9.42E-02
RNA-binding	AccD, RNA pol.	AT3G52150	CP	NA	RNA-binding (RRM/RBD/RNP motifs) family protein	2.33	0.87	1.65E-03		4.25E-02
$\mathbb{Z}$	RNA pol., Ribo.	AT3G23700	CP	NA	Nucleic acid-binding proteins superfamily	0.40	0.68	2.82E-02		8.82E-03
1	RNA pol.**	AT1G12800	CP	NA	Nucleic acid-binding, OB-fold-like protein	0.25	0.70	3.12E-02	4.50E-02	2.12E-02
	RNA pol.	AT2G20020	CP	CAF1, ATCAF1	RNA-binding CRS1 / YhbY (CRM) domain-containing protein	0.72	0.61	3.40E-02	2.84E-01	4.68E-02
	AccD	AT5G14580	MT	NA	polyribonucleotide nucleotidyltransferase, putative	9.88	0.62	6.86E-02	2.18E-13	9.07E-02
	AccD, ClpP1, RNA pol.	AT1G06950	CP	ATTIC110, TIC110	translocon at the inner envelope membrane of chloroplasts 110	5.77	0.79	3.45E-03	5.53E-01	1.42E-02
Import	Ycf1/2, RNA pol.*	AT5G22640	СР	emb1211	MORN (Membrane Occupation and Recognition Nexus) repeat-containing protein	1.72	0.91	3.45E-04	1.12E-01	1.43E-03
	AccD**	AT5G03940	CP	FFC, 54CP, CPSRP54, SRP54CP	chloroplast signal recognition particle 54 kDa subunit	15.57	0.82	1.65E-03	5.53E-01	3.84E-02

Ribo., Phot., RNA pol.	AT4G26670	Dual	NA	NA Mitochondrial import inner membrane translocase subunit Tim17/Tim22/Tim23 family protein		0.72	5.14E-03	6.85E-01	7.42E-01
Ribo.	AT3G23710	CP	NA	Tic22-like family protein	0.47	0.75	9.53E-03	2.91E-01	5.87E-01
Phot.	AT3G04340	CP	FTSHi5	FTSH protease-like 5	0.09	0.71	4.89E-02	8.98E-01	1.37E-01
Ycf1/2**	AT1G79560		EMB156, EMB36, EMB1047, FTSH12	FTSH protease 12	3.31	0.87	7.86E-04	2.73E-01	2.09E-02

**Table 2: Strong ERC hits lacking organelle-localized annotation.** AGI locus identifiers are shown for nuclear genes with significant ERC with plastome partition(s). \* indicates significant ERC for the partition in multiple regression. \*\* indicates the shown partition was the only significant ERC under multiple regression. For genes that are hits in multiple plastome partitions, the Slope, R<sup>2</sup>, and P-values for partition with the lowest Pearson P-value are reported. *O. sativa* IDs are shown for families in which *A. thaliana* is not present. One ERC hit lacking an *A. thaliana* and *O. sativa* ID was omitted. For full results see Supplementary Data.

DI i						4 1' D	4 1' D	
Plastome partition	AGI locus	Gene symbol	TAIR description	Slope	R <sup>2</sup>	Adj. P (Pearson)	Adj. P (Spearman)	Mult. reg. P
AccD*	AT5G59860	NA	RNA-binding (RRM/RBD/RNP motifs) family protein	1.29	0.94	6.07E-04	6.51E-01	7.41E-06
AccD*	AT1G16750	NA	Protein of unknown function, DUF547	2.18	0.94	1.65E-03	6.91E-01	3.32E-03
Ycf1/2	AT1G04110	SDD1	Subtilase family protein (		0.94	1.71E-03	3.63E-01	1.66E-02
Ycf1/2**	AT5G22450	NA	unknown protein	1.68	0.81	8.14E-03	1.92E-01	6.25E-02
RNA pol.*	OS03G58204	NA	NA	0.39	0.75	8.50E-03	1.97E-01	6.91E-03
Ribo.	AT4G14100	NA	transferases, transferring glycosyl groups	0.41	0.67	1.02E-02	7.52E-01	4.74E-01
RNA pol.	AT3G26618	ERF1-3	eukaryotic release factor 1-3	0.54	0.68	1.08E-02	7.37E-01	6.40E-01
ClpP1**	AT1G09800	NA	Pseudouridine synthase family protein	5.28	0.74	1.23E-02	5.69E-01	1.53E-03
Ycf1/2	AT4G25320	NA	AT hook motif DNA-binding family protein	0.75	0.75	2.22E-02	2.66E-01	2.61E-02
Ycf1/2	OS03G53360	NA	NA	1.59	0.88	2.22E-02	2.19E-01	2.14E-01
AccD	AT5G36000	NA	BEST A.thaliana match: reduced male fertility	0.18	0.80	2.65E-02	5.53E-01	8.69E-03
Ycf1/2*	AT1G55870	ATPARN, AHG2	Polynucleotidyl transferase, ribonuclease H-like superfamily protein	2.61	0.73	2.85E-02	3.37E-01	4.26E-03
ClpP1**	AT2G16770	bZIP23	Basic-leucine zipper (bZIP) transcription factor family protein	4.48	0.63	3.05E-02	7.41E-01	9.04E-04
RNA pol., AccD, Ribo.	AT4G19985	NA	Acyl-CoA N-acyltransferases (NAT) superfamily protein		0.66	3.20E-02	4.10E-01	7.14E-01
RNA pol.	AT1G69410	ATELF5A-3, ELF5A-3	eukaryotic elongation factor 5A-3		0.61	3.20E-02	8.76E-01	4.79E-01
RNA pol.	AT3G17880	HIP, ATTDX, ATHIP2, TDX	tetraticopeptide domain-containing thioredoxin	0.11	0.62	3.37E-02	7.47E-01	8.60E-02
AccD	AT4G19350	EMB3006	embryo defective 3006	1.88	0.75	3.42E-02	7.16E-01	1.97E-02
Ycf1/2**	OS03G26080	NA	NA	4.10	0.71	3.50E-02	2.20E-01	1.17E-01
RNA pol.	AT5G25840	NA	Protein of unknown function (DUF1677)	0.45	0.63	3.54E-02	2.60E-01	1.98E-01
RNA pol.	AT4G39920	POR, TFCC	C-CAP/cofactor C-like domain- containing protein	0.36	0.65	3.71E-02	5.08E-01	2.94E-01
Ribo., RNA pol.	AT1G71000	NA	Chaperone DnaJ-domain superfamily protein	0.62	0.62	3.93E-02	5.96E-01	5.68E-01
AccD	AT5G39420	cdc2cAt	CDC2C	4.59	0.74	3.95E-02	6.58E-01	4.11E-01
RNA pol.	AT1G03330	NA	Small nuclear ribonucleoprotein family protein	0.69	0.77	4.27E-02	2.18E-01	1.83E-01
Ribo.	AT2G03820	NA	nonsense-mediated mRNA decay NMD3 family protein	0.19	0.59	4.34E-02	7.52E-01	1.06E-01
RNA pol.	AT5G26610	NA	D111/G-patch domain-containing protein		0.58	4.49E-02	5.07E-01	5.88E-01
Phot., RNA pol.	AT5G20040	IPT9	isopentenyltransferase 9		0.63	4.74E-02	1.70E-01	1.61E-02
AccD	AT5G52860	ABCG8	ABC-2 type transporter family protein		0.57	1.16E-01	2.18E-13	6.62E-02
AccD	AT2G28315	NA	Nucleotide/sugar transporter family protein	6.45	0.63	1.17E-01	2.18E-13	1.53E-01
AccD	OS09G39370	NA	NA	1.68	0.59	2.70E-01	2.18E-13	1.51E-01
MatK	AT4G23330	NA	BEST A. thaliana match: eukaryotic ranslation initiation factor 3A		0.43	3.96E-01	2.91E-13	5.69E-01

Table S1. Proteome data sources.

Species	Lineage	Plastome rate	Dataset Type	Nuclear data source	Plastome NCBI accession
Arabidopsis thaliana	Eudicot (rosid)	Slow	Genome	TAIR (version Araport11)	NC_000932.1
Amborella trichopoda	Amborellales	Slow	Genome	Phytozome (version 12)	NC_005086.1
Cucumis sativus	Eudicot (rosid)	Slow	Genome	Phytozome (version 12)	NC_007144.1
Eucalyptus grandis	Eudicot (rosid)	Slow	Genome	Phytozome (version 12)	NC_014570.1
Gossypium raimondii	Eudicot (rosid)	Slow	Genome	Phytozome (version 12)	NC_016668.1
Musa acuminata	Monocot	Slow	Genome	Phytozome (version 12)	HF677508.1
Oryza sativa	Monocot	Fast	Genome	Phytozome (version 12)	NC_001320.1
Populus trichocarpa	Eudicot (rosid)	Slow	Genome	Phytozome (version 12)	NC_009143.1
Prunus persica	Eudicot (rosid)	Slow	Genome	Phytozome (version 12)	NC_014697.1
Solanum lycopersicum	Eudicot (asterid)	Slow	Genome	Phytozome (version 12)	NC_007898.3
Vitis vinifera	Eudicot (rosid)	Slow	Genome	Phytozome (version 12)	NC_015891.1
Spirodela polyrhiza	Monocot	Slow	Genome	Phytozome (version 12)	NC_015891.1
Helianthus annuus	Eudicot (asterid)	Slow	Genome	https://sunflowergenome .org	NC_007977.1
Lobelia siphilitica	Eudicot (asterid)	Fast	Transcriptome	1000 Plant Transcriptome Initiative	KY354225.1
Oenothera biennis	Eudicot (rosid)	Fast	Transcriptome	1000 Plant Transcriptome Initiative	NC_010361.1
Plantago maritima	Eudicot (asterid)	Fast	Transcriptome	1000 Plant Transcriptome Initiative	NC_028519.1
Acacia aulacocarpa/ligulata	Eudicot (rosid)	Fast	Transcriptome	PlanTransDB	NC_026134.2
Geranium maderense	Eudicot (rosid)	Fast	Transcriptome	PlanTransDB	NC_029999.1
Liriodendron chinense	Magnoliid	Slow	Transcriptome	Yang et al., 2014	NC_030504.1
Silene noctiflora	Eudicot (caryophyllid)	Fast	Transcriptome	Sloan et al., 2014b	NC_016728.1

**Table S2: Plastome partition multiple sequence alignments.** Information about plastome partitions used to infer plastid trees.

Plastome partition	Number of genes	Gene(s)	Alignment length (AAs)	Missing species
AccD	1	AccD	1281	Oryza sativa and Lobelia siphilitica
ClpP1	1	ClpP1	177	NA
MatK	1	MatK	458	NA
Photosynthesis	46	AtpA, AtpB, AtpE, AtpF, AtpH, AtpI, NdhA, NdhB, NdhC, NdhD, NdhE, NdhF, NdhG, NdhH, NdhI, NdhJ, NdhK, PetA, PetB, PetD, PetG, PetL, PetN, PsaA, PsaB, PsaC, PsaI, PsaJ, PsbA, PsbB, PsbC, PsbD, PsbE, PsbF, PsbH, PsbI, PsbJ, PsbK, PsbL, PsbM, PsbN, PsbT, PsbZ, RbcL, Ycf3, Ycf4	10437	NA
Ribosomes	20	Rpl14, Rpl16, Rpl2, Rpl20, Rpl22, Rpl32, Rpl33, Rpl36, Rps11, Rps12, Rps14, Rps15, Rps16, Rps18, Rps19, Rps2, Rps3, Rps4, Rps7, Rps8	2492	NA
RNA pol.	4	RpoA, RpoB, RpoC1, RpoC2	3209	NA
Ycf1/Ycf2	2	Ycf1, Ycf2	2479	Oryza sativa and Geranium maderense

**Table S3. ERC hits identified for each plastome partition.** Number of hits designated for each partition according to different thresholds referenced throughout the manuscript. *Single correlation* hits were used in Fig. 4 and 5. *Single correlation (strong hits)* were used for Table 1 and 2. *Multiple regression* hits were used in Fig. S3C-F.

	AccD	ClpP1	MatK	Phot.	Ribo.	RNA pol.	Ycf1/2
Single correlation	514	371	333	324	322	289	284
Single correlation (strong hits)	48	21	6	33	59	60	38
Multiple regression	159	182	131	160	118	303	226

Table S4. ERC comparisons among the seven plastome partitions.  $R^2$  values (top) and Pearson p-values (bottom in parentheses) for the ERC comparisons of plastome partitions to each other. All p-values remained significant (p  $\leq$  0.05) after FDR correction using the p-values posted in this table.

	AccD	ClpP1	MatK	Phot.	Ribo.	RNA pol.	Ycf1/2
AccD	-	-	-	-	-	-	-
ClpP1	0.58 (5.92E-04)	-	-	-	-	-	-
MatK	0.27 (3.77E-02)	0.25 (3.41E-02)	-	-	-	-	-
Phot.	0.64 (1.94E-04)	0.37 (7.63E-03)	0.74 (4.90E-06)	-	-	1	1
Ribo.	0.72 (3.06E-05)	0.50 (9.61E-04)	0.51 (8.50E-04)	0.83 (1.64E-07)	-	-	-
RNA pol.	0.70 (5.55E-05)	0.38 (6.29E-03)	0.41 (4.26E-03)	0.65 (5.24E-05)	0.82 (2.55E-07)	-	-
Ycf1/2	0.79 (9.94E-06)	0.40 (9.11E-03)	0.33 (1.91E-02)	0.68 (9.06E-05)	0.79 (3.72E-06)	0.64 (1.85E-04)	-

## **References:**

701

702

703

- Adam, Z., Aviv-Sharon, E., Keren-Paz, A., Naveh, L., Rozenberg, M., Savidor, A., & Chen, J.
- 671 (2019). The chloroplast envelope protease FTSH11 Interaction with CPN60 and
- identification of potential substrates. Frontiers in Plant Science, 10(April), 1–11.
- https://doi.org/10.3389/fpls.2019.00428
- Bansal, M. S., & Eulenstein, O. (2008). The multiple gene duplication problem revisited. *Bioinformatics (Oxford, England)*, 24(13), i132-8.
- https://doi.org/10.1093/bioinformatics/btn150
- Barnard-Kubow, K. B., So, N., & Galloway, L. F. (2016). Cytonuclear incompatibility contributes to the early stages of speciation. *Evolution*, 70(12), 2752–2766. https://doi.org/10.1111/evo.13075
- 680 Bieri, P., Leibundgut, M., Saurer, M., Boehringer, D., & Ban, N. (2017). The complete structure 681 of the chloroplast 70S ribosome in complex with translation factor pY. *The EMBO Journal*, 682 36(4), 475–486. https://doi.org/10.15252/embj.201695959
- Birchler, J. A., & Veitia, R. A. (2012). Gene balance hypothesis: Connecting issues of dosage
   sensitivity across biological disciplines. *Proceedings of the National Academy of Sciences* of the United States of America, 109(37), 14746–14753.
   https://doi.org/10.1073/pnas.1207726109
- Boerema, A. P., Aibara, S., Paul, B., Tobiasson, V., Kimanius, D., Forsberg, B. O., Wallden, K., Lindahl, E., & Amunts, A. (2018). Structure of the chloroplast ribosome with chl-RRF and hibernation-promoting factor. *Nature Plants*, *4*(4), 212–217. https://doi.org/10.1038/s41477-018-0129-6
- Bogdanova, V. S., Zaytseva, O. O., Mglinets, A. V., Shatskaya, N. V., Kosterin, O. E., &
   Vasiliev, G. V. (2015). Nuclear-cytoplasmic conflict in pea (Pisum sativum L.) is associated
   with nuclear and plastidic candidate genes encoding acetyl-coA carboxylase subunits. *PLoS ONE*, *10*(3), 1–18. https://doi.org/10.1371/journal.pone.0119835
- Bonen, L., & Calixte, S. (2005). Comparative aqualysis of bacterial-origin genes for plant
   mitochondrial ribosomal proteins. *Mol Biol Evol*, 23(3), 701–712.
   https://doi.org/10.1093/molbev/msj080
- 698 Castresana, J. (2000). Selection of conserved blocks from multiple alignments for their use in 699 phylogenetic analysis. *Molecular Biology and Evolution*, 17(4), 540–552. 700 https://doi.org/10.1093/oxfordjournals.molbev.a026334
  - Cho, Y., Mower, J. P., Qiu, Y. L., & Palmer, J. D. (2004). Mitochondrial substitution rates are extraordinarily elevated and variable in a genus of flowering plants. *Proceedings of the National Academy of Sciences of the United States of America*, 101(51), 17741–17746. https://doi.org/10.1073/pnas.0408302101
- Christian, R. W., Hewitt, S. L., Roalson, E. H., & Dhingra, A. (2020). Genome-Scale
   Characterization of Predicted Plastid-Targeted Proteomes in Higher Plants. Scientific
   Reports, 10(1), 1–22. https://doi.org/10.1038/s41598-020-64670-5
- Clark, Nathan L, Alani, E., & Aquadro, C. F. (2012). Evolutionary Rate Covariation: A
   bioinformatic method that reveals co-functionality and co-expression of genes. *Genome Research*, 22(607), 714–720. https://doi.org/10.1101/gr.132647.111.Guerois
- Clark, Nathaniel L., & Aquadro, C. F. (2010). A novel method to detect proteins evolving at correlated rates: Identifying new functional relationships between coevolving proteins.

713 *Molecular Biology and Evolution*, *27*(5), 1152–1161. 714 https://doi.org/10.1093/molbev/msp324

733

734

735

- Colombo, M., Tadini, L., Peracchio, C., Ferrari, R., & Pesaresi, P. (2016). GUN1, a jack-of-all-trades in chloroplast protein homeostasis and signaling. *Frontiers in Plant Science*,
   7(September). https://doi.org/10.3389/fpls.2016.01427
- Conway, J. R., Lex, A., & Gehlenborg, N. (2017). UpSetR: An R package for the visualization of intersecting sets and their properties. *Bioinformatics*, 33(18), 2938–2940. https://doi.org/10.1093/bioinformatics/btx364
- Costello, R., Emms, D. M., & Kelly, S. (2020). Gene duplication accelerates the pace of protein gain and loss from plant organelles. *Molecular Biology and Evolution*, *37*(4), 969–981. https://doi.org/10.1093/molbev/msz275
- Couvillion, M. T., Soto, I. C., Shipkovenska, G., & Churchman, L. S. (2016). Synchronized
   mitochondrial and cytosolic translation programs. *Nature*, *533*(7604), 499–503.
   https://doi.org/10.1038/nature18015
- 727 Creff, A., Sormani, R., & Desnos, T. (2010). The two Arabidopsis RPS6 genes, encoding for 728 cytoplasmic ribosomal proteins S6, are functionally equivalent. *Plant Molecular Biology*, 729 73(4), 533–546. https://doi.org/10.1007/s11103-010-9639-y
- De Juan, D., Pazos, F., & Valencia, A. (2013). Emerging methods in protein co-evolution.
   Nature Reviews Genetics, 14(4), 249–261. https://doi.org/10.1038/nrg3414
   De Smet, R., Adams, K. L., Vandepoele, K., Van Montagu, M. C. E., Maere, S., & Van de
  - De Smet, R., Adams, K. L., Vandepoele, K., Van Montagu, M. C. E., Maere, S., & Van de Peer, Y. (2013). Convergent gene loss following gene and genome duplications creates single-copy families in flowering plants. *Proceedings of the National Academy of Sciences of the United States of America*, 110(8), 2898–2903. https://doi.org/10.1073/pnas.1300127110/-/DCSupplemental.www.pnas.org/cgi/doi/10.1073/pnas.1300127110
- Degnan, J. H., & Rosenberg, N. a. (2009). Gene tree discordance, phylogenetic inference and the multispecies coalescent. *Trends in Ecology & Evolution*, 24(6), 332–340. https://doi.org/10.1016/j.tree.2009.01.009
- Dogra, V., Duan, J., Lee, K. P., & Kim, C. (2019). Impaired PSII proteostasis triggers a UPR-like response in the var2 mutant of Arabidopsis. *Journal of Experimental Botany*, 70(12), 3075–3088. https://doi.org/10.1093/jxb/erz151
- Duarte, J. M., Wall, P. K., Edger, P. P., Landherr, L. L., Ma, H., Pires, J. C., Leebens-Mack, J.,
   & dePamphilis, C. W. (2010). Identification of shared single copy nuclear genes in
   Arabidopsis, Populus, Vitis and Oryza and their phylogenetic utility across various
   taxonomic levels. *BMC Evolutionary Biology*, 10, 61. https://doi.org/10.1186/1471-2148 10-61
- Dugas, D. V., Hernandez, D., Koenen, E. J. M., Schwarz, E., Straub, S., Hughes, C. E., Jansen,
   R. K., Nageswara-Rao, M., Staats, M., Trujillo, J. T., Hajrah, N. H., Alharbi, N. S., Al Malki, A. L., Sabir, J. S. M., & Bailey, C. D. (2015). Mimosoid legume plastome evolution:
   IR expansion, tandem repeat expansions, and accelerated rate of evolution in clpP. *Scientific Reports*, 5(October), 1–13. https://doi.org/10.1038/srep16958
- Emms, D. M., & Kelly, S. (2015). OrthoFinder: solving fundamental biases in whole genome
   comparisons dramatically improves orthogroup inference accuracy. *Genome Biology*, 16(1),
   157. https://doi.org/10.1186/s13059-015-0721-2
- Felsenstein, J. (1985). Phylogenies and the comparative method. *American Naturalist*, 125(1), 1–15. https://doi.org/10.1086/284325
- 758 Ferro, M., Brugière, S., Salvi, D., Seigneurin-Berny, D., Court, M., Moyet, L., Ramus, C., Miras,

- S., Mellal, M., Le Gall, S., Kieffer-Jaquinod, S., Bruley, C., Garin, J., Joyard, J., Masselon,
   C., & Rolland, N. (2010). AT-CHLORO, a comprehensive chloroplast proteome database
   with subplastidial localization and curated information on envelope proteins. *Molecular and Cellular Proteomics*, 9(6), 1063–1084. https://doi.org/10.1074/mcp.M900325-MCP200
- Ferro, M., Salvi, D., Brugière, S., Miras, S., Kowalski, S., Louwagie, M., Garin, J., Joyard, J., &
   Rolland, N. (2003). Proteomics of the chloroplast envelope membranes from Arabidopsis
   thaliana. *Molecular & Cellular Proteomics : MCP*, 2(5), 325–345.
   https://doi.org/10.1074/mcp.M300030-MCP200
- Findlay, G. D., Sitnik, J. L., Wang, W., Aquadro, C. F., Clark, N. L., & Wolfner, M. F. (2014).
   Evolutionary Rate Covariation Identifies New Members of a Protein Network Required for
   Drosophila melanogaster Female Post-Mating Responses. *PLoS Genetics*, 10(1).
   https://doi.org/10.1371/journal.pgen.1004108

771

772

773

774

775

776

777

778

779

780

781

782

783

784

785

786

- Forsythe, E. S., Nelson, A. D. L., & Beilstein, M. A. (2020). Biased gene retention in the face of introgression obscures species relationships. *Genome Biology and Evolution*, 1–44.
- Forsythe, E. S., Sharbrough, J., Havird, J. C., Warren, J. M., & Sloan, D. B. (2019). CyMIRA: The Cytonuclear Molecular Interactions Reference for Arabidopsis. *Genome Biology and Evolution*, 11(8), 2194–2202. https://doi.org/10.1093/gbe/evz144
- Goh, C. S., Bogan, A. A., Joachimiak, M., Walther, D., & Cohen, F. E. (2000). Co-evolution of proteins with their interaction partners. *Journal of Molecular Biology*, 299(2), 283–293. https://doi.org/10.1006/jmbi.2000.3732
- Gould, S. B., Waller, R. F., & McFadden, G. I. (2008). Plastid Evolution. *Annual Review of Plant Biology*, 59(1), 491–517. https://doi.org/10.1146/annurev.arplant.59.032607.092915
- Greiner, S., Rauwolf, U., Meurer, J., & Herrmann, R. G. (2011). The role of plastids in plant speciation. *Molecular Ecology*, 20(4), 671–691. https://doi.org/10.1111/j.1365-294X.2010.04984.x
- Guisinger, M. M., Kuehl, J. V., Boore, J. L., & Jansen, R. K. (2008). Genome-wide analyses of Geraniaceae plastid DNA reveal unprecedented patterns of increased nucleotide substitutions. *Proceedings of the National Academy of Sciences of the United States of America*, 105(47), 18424–18429. https://doi.org/10.1073/pnas.0806759105
- Guisinger, M. M., Kuehl, J. V., Boore, J. L., & Jansen, R. K. (2011). Extreme reconfiguration of plastid genomes in the angiosperm family Geraniaceae: Rearrangements, repeats, and codon usage. *Molecular Biology and Evolution*, 28(1), 583–600.
   https://doi.org/10.1093/molbev/msq229
- Heinemann, B., Künzler, P., Braun, H.-P., & Hildebrandt, T. (2020). Estimating the number of protein molecules in a plant cell: a quantitative perspective on proteostasis and amino acid homeostasis during progressive drought stress. *Plant Physiology*. https://doi.org/10.1101/2020.03.17.995613
- Hilu, K. W., Borsch, T., Müller, K., Soltis, D. E., Soltis, P. S., Savolainen, V., Chase, M. W.,
  Powell, M. P., Alice, L. A., Evans, R., Sauquet, H., Neinhuis, C., Slotta, T. A. B., Rohwer,
  J. G., Campbell, C. S., & Chatrou, L. W. (2003). Angiosperm phylogeny based on matk
  sequence information. *American Journal of Botany*, 90(12), 1758–1776.
  https://doi.org/10.3732/ajb.90.12.1758
- Houtkooper, R. H., Mouchiroud, L., Ryu, D., Moullan, N., Katsyuba, E., Knott, G., Williams, R. W., & Auwerx, J. (2013). Mitonuclear protein imbalance as a conserved longevity mechanism. *Nature*, 497(7450), 451–457. https://doi.org/10.1038/nature12188
- Jansen, R. K., Cai, Z., Raubeson, L. A., Daniell, H., Depamphilis, C. W., Leebens-Mack, J.,

- Müller, K. F., Guisinger-Bellian, M., Haberle, R. C., Hansen, A. K., Chumley, T. W., Lee, S. B., Peery, R., McNeal, J. R., Kuehl, J. V., & Boore, J. L. (2007). Analysis of 81 genes from 64 plastid genomes resolves relationships in angiosperms and identifies genome-scale evolutionary patterns. *Proceedings of the National Academy of Sciences of the United States of America*, 104(49), 19369–19374. https://doi.org/10.1073/pnas.0709121104
- Katoh, K., & Standley, D. M. (2013). MAFFT multiple sequence alignment software version 7: Improvements in performance and usability. *Molecular Biology and Evolution*, 30(4), 772–780. https://doi.org/10.1093/molbev/mst010
- Kikuchi, S., Asakura, Y., Imai, M., Nakahira, Y., Kotani, Y., Hashiguchi, Y., Nakai, Y.,
  Takafuji, K., Bédard, J., Hirabayashi-Ishioka, Y., Mori, H., Shiina, T., & Nakai, M. (2018).
  A Ycf2-FtsHi heteromeric AAA-ATPase complex is required for chloroplast protein
  import. *Plant Cell*, 30(11), 2677–2703. https://doi.org/10.1105/tpc.18.00357
- Kim, J., Olinares, P. D., Oh, S. H., Ghisaura, S., Poliakov, A., Ponnala, L., & van Wijk, K. J. (2013). Modified Clp protease complex in the ClpP3 null mutant and consequences for chloroplast development and function in Arabidopsis. *Plant Physiology*, *162*(1), 157–179. https://doi.org/10.1104/pp.113.215699

821

822

823

824

825

826

827

828

- Knox, E. B. (2014). The dynamic history of plastid genomes in the Campanulaceae sensu lato is unique among angiosperms. *Proceedings of the National Academy of Sciences of the United States of America*, 111(30), 11097–11102. https://doi.org/10.1073/pnas.1403363111
- Leebens-Mack, Barker, Carpenter, et al. (2019). *One thousand plant transcriptomes and the phylogenomics of green plants*. *16*(November 2017). https://doi.org/10.1038/s41586-019-1693-2
- Liu, X., Yu, F., & Rodermel, S. (2010). An arabidopsis pentatricopeptide repeat protein, SUPPRESSOR OF VARIEGATION7, is required for FtsH-mediated chloroplast biogenesis. *Plant Physiology*, 154(4), 1588–1601. https://doi.org/10.1104/pp.110.164111
- Madaoui, H., & Guerois, R. (2008). Coevolution at protein complex interfaces can be detected by the complementarity trace with important impact for predictive docking. *Proceedings of the National Academy of Sciences of the United States of America*, 105(22), 7708–7713. https://doi.org/10.1073/pnas.0707032105
- Magee, A. M., Aspinall, S., Rice, D. W., Cusack, B. P., Sémon, M., Perry, A. S., Stefanović, S.,
  Milbourne, D., Barth, S., Palmer, J. D., Gray, J. C., Kavanagh, T. A., & Wolfe, K. H.
  (2010). Localized hypermutation and associated gene losses in legume chloroplast genomes. *Genome Research*, 20(12), 1700–1710. https://doi.org/10.1101/gr.111955.110
- Millar, A. H., Whelan, J., & Small, I. (2006). Recent surprises in protein targeting to
   mitochondria and plastids. *Current Opinion in Plant Biology*, 9(6), 610–615.
   https://doi.org/10.1016/j.pbi.2006.09.002
- Molina, J., Hazzouri, K. M., Nickrent, D., Geisler, M., Meyer, R. S., Pentony, M. M., Flowers, J.
  M., Pelser, P., Barcelona, J., Inovejas, S. A., Uy, I., Yuan, W., Wilkins, O., Michel, C. I.,
  Locklear, S., Concepcion, G. P., & Purugganan, M. D. (2014). Possible loss of the
  chloroplast genome in the parasitic flowering plant Rafflesia lagascae (Rafflesiaceae).
  Molecular Biology and Evolution, 31(4), 793–803. https://doi.org/10.1093/molbev/msu051
- Mower, J. P., Touzet, P., Gummow, J. S., Delph, L. F., & Palmer, J. D. (2007). Extensive
   variation in synonymous substitution rates in mitochondrial genes of seed plants. *BMC Evolutionary Biology*, 7, 1–14. https://doi.org/10.1186/1471-2148-7-135
- Nevill, P. G., Howell, K. A., Cross, A. T., Williams, A. V., Zhong, X., Tonti-Filippini, J., Boykin, L. M., Dixon, K. W., & Small, I. (2019). Plastome-wide rearrangements and gene

losses in carnivorous droseraceae. *Genome Biology and Evolution*, 11(2), 472–485. https://doi.org/10.1093/gbe/evz005

861

862

863

864

865

866

867

868

869

870

885

886

- Nishimura, K., & van Wijk, K. J. (2015). Organization, function and substrates of the essential Clp protease system in plastids. *BBA Bioenergetics*, *1847*(9), 915–930. https://doi.org/10.1016/j.bbabio.2014.11.012
- Ovchinnikov, S., Kamisetty, H., & Baker, D. (2014). Robust and accurate prediction of residueresidue interactions across protein interfaces using evolutionary information. *ELife*, 2014(3), 1–21. https://doi.org/10.7554/eLife.02030
- Panchy, N., Lehti-Shiu, M., & Shiu, S. H. (2016). Evolution of gene duplication in plants. *Plant Physiology*, *171*(4), 2294–2316. https://doi.org/10.1104/pp.16.00523
  - Paradis, E., Claude, J., & Strimmer, K. (2004). APE: Analyses of phylogenetics and evolution in R language. *Bioinformatics*, 20(2), 289–290. https://doi.org/10.1093/bioinformatics/btg412
  - Park, Seongjun, Ruhlman, T. A., Weng, M. L., Hajrah, N. H., Sabir, J. S. M., & Jansen, R. K. (2017). Contrasting patterns of nucleotide substitution rates provide insight into dynamic evolution of plastid and mitochondrial genomes of Geranium. *Genome Biology and Evolution*, *9*(6), 1766–1780. https://doi.org/10.1093/gbe/evx124
  - Park, Sungsoon, & Rodermel, S. R. (2004). Mutations in ClpC2/Hsp100 suppress the requirement for FtsH in thylakoid membrane biogenesis. *Proceedings of the National Academy of Sciences of the United States of America*, 101(34), 12765–12770. https://doi.org/10.1073/pnas.0402764101
- Parkinson, C. L., Mower, J. P., Qiu, Y. L., Shirk, A. J., Song, K., Young, N. D., DePamphilis, C. W., & Palmer, J. D. (2005). Multiple major increases and decreases in mitochondrial substitution rates in the plant family Geraniaceae. *BMC Evolutionary Biology*, *5*, 1–12. https://doi.org/10.1186/1471-2148-5-73
- Qiu, Y. L., Dombrovska, O., Lee, J., Li, L., Whitlock, B. A., Bernasconi-Quadroni, F., Rest, J.
  S., Davis, C. C., Borsch, T., Hilu, K. W., Renner, S. S., Soltis, D. E., Soltis, P. S., Zanis, M.
  J., Cannone, J. J., Gutell, R. R., Powell, M., Savolainen, V., Chatrou, L. W., & Chase, M.
  W. (2005). Phylogenetic analyses of basal angiosperms based on nine plastid,
  mitochondrial, and nuclear genes. *International Journal of Plant Sciences*, 166(5), 815–842.
  https://doi.org/10.1086/431800
- Qiu, Y. L., Li, L., Hendry, T. A., Li, R., Taylor, D. W., Issa, M. J., Ronen, A. J., Vekaria, M. L.,
  & White, A. M. (2006). Reconstructing the basal angiosperm phylogeny: Evaluating
  information content of mitochondrial genes. *Taxon*, 55(4), 837–856.
  https://doi.org/10.2307/25065680
  - Ramani, A. K., & Marcotte, E. M. (2003). Exploiting the co-evolution of interacting proteins to discover interaction specificity. *Journal of Molecular Biology*, *327*(1), 273–284. https://doi.org/10.1016/S0022-2836(03)00114-1
- Raza, Q., Choi, J. Y., Li, Y., O'Dowd, R. M., Watkins, S. C., Chikina, M., Hong, Y., Clark, N.
  L., & Kwiatkowski, A. V. (2019). Evolutionary rate covariation analysis of E-cadherin identifies Raskol as a regulator of cell adhesion and actin dynamics in Drosophila. *PLoS Genetics*, 15(2), 1–24. https://doi.org/10.1371/journal.pgen.1007720
- Rockenbach, K., Havird, J. C., Grey Monroe, J., Triant, D. A., Taylor, D. R., & Sloan, D. B. (2016). Positive selection in rapidly evolving plastid-nuclear enzyme complexes. *Genetics*, 204(4), 1507–1522. https://doi.org/10.1534/genetics.116.188268
- Sanderson, M. J., & McMahon, M. M. (2007). Inferring angiosperm phylogeny from EST data with widespread gene duplication. *BMC Evolutionary Biology*, *7 Suppl 1*, S3.

897 https://doi.org/10.1186/1471-2148-7-S1-S3

911

912

913

914

915

916

917

918

919

920

921

922

923

924

925

926

927

928

929

- Sangiovanni, M., Vigilante, A., & Chiusano, M. (2013). Exploiting a Reference Genome in Terms of Duplications: The Network of Paralogs and Single Copy Genes in Arabidopsis thaliana. *Biology*, 2(4), 1465–1487. https://doi.org/10.3390/biology2041465
- Sato, T., Yamanishi, Y., Kanehisa, M., & Toh, H. (2005). The inference of protein-protein interactions by co-evolutionary analysis is improved by excluding the information about the phylogenetic relationships. *Bioinformatics*, 21(17), 3482–3489. https://doi.org/10.1093/bioinformatics/bti564
- Schmitz-Linneweber, C., Kushnir, S., Babiychuk, E., Poltnigg, P., Herrmann, R. G., & Maier, R.
   M. (2005). Pigment deficiency in nightshade/tobacco cybrids is caused by the failure to edit the plastid ATPase α-subunit mRNA. *Plant Cell*, 17(6), 1815–1828.
   https://doi.org/10.1105/tpc.105.032474
- 909 Sharbrough, J., Conover, J. L., Tate, J. A., Wendel, J. F., & Sloan, D. B. (2017). *Cytonuclear responses to genome doubling*. *104*(9), 1–4. https://doi.org/10.3732/ajb.1700293
  - Shrestha, B., Weng, M. L., Theriot, E. C., Gilbert, L. E., Ruhlman, T. A., Krosnick, S. E., & Jansen, R. K. (2019). Highly accelerated rates of genomic rearrangements and nucleotide substitutions in plastid genomes of Passiflora subgenus Decaloba. *Molecular Phylogenetics and Evolution*, 138(May), 53–64. https://doi.org/10.1016/j.ympev.2019.05.030
  - Sloan, D. B., Oxelman, B., Rautenberg, A., & Taylor, D. R. (2009). Phylogenetic analysis of mitochondrial substitution rate variation in the angiosperm tribe Sileneae. *BMC Evolutionary Biology*, *9*(1), 1–16. https://doi.org/10.1186/1471-2148-9-260
  - Sloan, D. B., Triant, D. A., Forrester, N. J., Bergner, L. M., Wu, M., & Taylor, D. R. (2014). A recurring syndrome of accelerated plastid genome evolution in the angiosperm tribe Sileneae (Caryophyllaceae). *Molecular Phylogenetics and Evolution*, 72(1), 82–89. https://doi.org/10.1016/j.ympev.2013.12.004
  - Sloan, D. B., Triant, D. A., Wu, M., & Taylor, D. R. (2014). Cytonuclear interactions and relaxed selection accelerate sequence evolution in organelle ribosomes. *Molecular Biology and Evolution*, 31(3), 673–682. https://doi.org/10.1093/molbev/mst259
  - Smith, M. L., & Hahn, M. W. (2020). New approaches for inferring phylogenies in the presence of paralogs. *BioRxiv*, 1, 6–8. https://doi.org/10.16309/j.cnki.issn.1007-1776.2003.03.004
  - Sobanski, J., Giavalisco, P., Fischer, A., Kreiner, J. M., Walther, D., Aurel, M., Pellizzer, T., Golczyk, H., Obata, T., Bock, R., Sears, B. B., & Greiner, S. (2019). *Chloroplast competition is controlled by lipid biosynthesis in evening primroses*. *116*(12). https://doi.org/10.1073/pnas.1811661116
- 931 Soltis, P. S., Soltis, D. E., & Chase, M. W. (1999). Angiosperm phylogeny inferred from 932 multiple genes as a tool for comparative biology. *Nature*, 402(6760), 402–404. 933 https://doi.org/10.1038/46528
- 934 Stamatakis, A. (2014). RAxML version 8: a tool for phylogenetic analysis and post-analysis of large phylogenies. *Bioinformatics (Oxford, England)*, 30(9), 1312–1313. 936 https://doi.org/10.1093/bioinformatics/btu033
- 937 Stolzer, M., Lai, H., Xu, M., Sathaye, D., Vernot, B., & Durand, D. (2012). Inferring 938 duplications, losses, transfers and incomplete lineage sorting with nonbinary species trees. 939 *Bioinformatics*, 28(18), i409–i415. https://doi.org/10.1093/bioinformatics/bts386
- Tiller, N., Weingartner, M., Thiele, W., Maximova, E., & Scho, M. A. (2012). The plastidspecific ribosomal proteins of Arabidopsis thaliana can be divided into non-essential proteins and genuine ribosomal proteins. *The Plan Journal*, 69, 302–316.

943 https://doi.org/10.1111/j.1365-313X.2011.04791.x

962

963

964

965

966

967

968

969

970

- Timmis, J. N., Ayliff, M. A., Huang, C. Y., & Martin, W. (2004). Endosymbiotic gene transfer:
  Organelle genomes forge eukaryotic chromosomes. *Nature Reviews Genetics*, *5*(2), 123–
  135. https://doi.org/10.1038/nrg1271
- van Wijk, K. J., & Baginsky, S. (2011). Plastid proteomics in higher plants: Current state and future goals. *Plant Physiology*, *155*(4), 1578–1588. https://doi.org/10.1104/pp.111.172932
- Vernot, B., Stolzer, M., Goldman, A., & Durand, D. (2008). Reconciliation with non-binary
   species trees. *Journal of Computational Biology : A Journal of Computational Molecular* Cell Biology, 15(8), 981–1006. https://doi.org/10.1089/cmb.2008.0092
- Wagner, R., Aigner, H., & Funk, C. (2012). FtsH proteases located in the plant chloroplast.
   *Physiologia Plantarum*, 145(1), 203–214. https://doi.org/10.1111/j.1399-3054.2011.01548.x
- Waltz, F., Nguyen, T. T., Arrivé, M., Bochler, A., Chicher, J., Hammann, P., Kuhn, L.,
  Quadrado, M., Mireau, H., Yashem, Y., & Giegé, P. (2019). Small is big in Arabidopsis
  mitochondrial ribosome. *Nature Plants*, 5(January), 106–117.
  https://doi.org/10.1038/s41477-018-0339-y
- Wang, R., Zhao, J., Jia, M., Xu, N., Liang, S., Shao, J., Qi, Y., Liu, X., An, L., & Yu, F. (2018).
   Balance between cytosolic and chloroplast translation affects leaf variegation. *Plant Physiology*, 176(1), 804–818. https://doi.org/10.1104/pp.17.00673
  - Wendel, J. F., Lisch, D., Hu, G., & Mason, A. S. (2018). The long and short of doubling down: polyploidy, epigenetics, and the temporal dynamics of genome fractionation. *Current Opinion in Genetics and Development*, 49, 1–7. https://doi.org/10.1016/j.gde.2018.01.004
  - Weng, M., Ruhlman, T. A., & Jansen, R. K. (2016). *Plastid Nuclear Interaction and Accelerated Coevolution in Plastid Ribosomal Genes in Geraniaceae*. 8(6), 1824–1838. https://doi.org/10.1093/gbe/evw115
  - Wicke, S., Müller, K. F., DePamphilis, C. W., Quandt, D., Bellot, S., & Schneeweiss, G. M. (2016). Mechanistic model of evolutionary rate variation en route to a nonphotosynthetic lifestyle in plants. *Proceedings of the National Academy of Sciences of the United States of America*, 113(32), 9045–9050. https://doi.org/10.1073/pnas.1607576113
- Williams, A. M., Friso, G., Wijk, K. J. Van, & Sloan, D. B. (2019). Extreme variation in rates of
   evolution in the plastid Clp protease complex. *The Plan Journal*, 1–17.
   https://doi.org/10.1111/tpj.14208
- Wolfe, N. W., & Clark, N. L. (2015). ERC analysis: Web-based inference of gene function via
   evolutionary rate covariation. *Bioinformatics*, 31(23), 3835–3837.
   https://doi.org/10.1093/bioinformatics/btv454
- Yan, Z., Ye, G., & Werren, J. H. (2019). Evolutionary Rate Correlation between Mitochondrial Encoded and Mitochondria-Associated Nuclear-Encoded Proteins in Insects. *Molecular Biology and Evolution*, 36(5), 1022–1036. https://doi.org/10.1093/molbev/msz036
- Yu, F., Liu, X., Alsheikh, M., Park, S., & Rodermel, S. (2008). Mutations in SUPPRESSOR OF
   VARIEGATION1, a factor required for normal chloroplast translation, suppress var2 mediated leaf variegation in Arabidopsis. *The Plant Cell*, 20(July), 1786–1804.
   https://doi.org/10.1105/tpc.107.054965
- Zanis, M. J., Soltis, D. E., Soltis, P. S., Mathews, S., & Donoghue, M. J. (2002). The root of the
   angiosperms revisited. *Proceedings of the National Academy of Sciences of the United* States of America, 99(10), 6848–6853. https://doi.org/10.1073/pnas.092136399
- 288 Zhang, J., Ruhlman, T. A., Sabir, J., Blazier, J. C., & Jansen, R. K. (2015). Coordinated rates of

989 evolution between interacting plastid and nuclear genes in geraniaceae. The Plant Cell, 990 27(March), 563–573. https://doi.org/10.1105/tpc.114.134353 991 Zhang, J., Ruhlman, T. A., Sabir, J. S. M., Blazier, J. C., Weng, M., Park, S., & Jansen, R. K. 992 (2016). Coevolution between Nuclear-Encoded DNA Replication, Recombination, and Repair Genes and Plastid Genome Complexity. 8(3), 622–634. 993 994 https://doi.org/10.1093/gbe/evw033 995 Zheng, M., Liu, X., Liang, S., Fu, S., Qi, Y., Zhao, J., Shao, J., An, L., & Yu, F. (2016). 996 Chloroplast translation initiation factors regulate leaf variegation and development. *Plant* 997 Physiology, 172(2), 1117–1130. https://doi.org/10.1104/pp.15.02040 998 Zupoka, A., Kozula, D., Schöttlera, M. A., Niehörstera, J., Garbscha, F., Liereb, K., Malinovaa, 999 I., Bock, R., & Greiner, S. (2020). A photosynthesis operon in the chloroplast genome 1000 drives speciation in evening primroses. BioRvix.